PEOPLE'S DEMOCRATIC REPUBLIC OF ALGERIA
MINISTRY OF HIGHER EDUCATION AND SCIENTIFIC RESEARCH
SCIENTIFIC RESEARCH

MOHAMED BOUDIAF UNIVERSITY - M'SILA

FACULTY :TECHNOLOGY
DEPARTMENT: ELECTRONICS
DOMAIN: COLLEGE OF TECHNOLOGY
FIELD OF STUDY: AUTOMATIC
OPTION: AUTOMATIC AND SYSTEMES

THESIS SUBMITTED FOR THE ATTAINMENT
OF THE ACADEMIC MASTER'S DEGREE
BY:

SAOUCHI Louey
BELABBES Fares

TITLE

FUZZY - SMC - PI Regulator for Speed Control of the Doubly Fed Induction Machine

Defended before the jury composed of:

Dr.ROUABHI Riyadh	**Universityof M'sila**	**President**
Dr. HERIZI Abdelghafour	**University of M'sila**	**supervisor**
Dr. OUAGUENI Fayssal	**University of M'sila**	**Co- supervisor**
Dr. HELLALI Lallouani	**Universityof M'sila**	**Examiner**

Academic year: 2024 / 2025

Acknowledgements

At the conclusion of this work, we would first like to express our gratitude to Almighty God, who granted us the strength and determination to complete this work.

We extend our sincere thanks to **Dr. Herizi Abdelghafour** for his patience, dedication, and valuable guidance throughout the preparation of our graduation project.

We also express our deep gratitude to **Dr. OUAGUENI Fayssal** for his continuous support and inspiring presence.

We deeply appreciate the support and guidance they provided, which had a significant impact on our success.

for his valuable advice, which enriched our thinking and guided this work

We also thank the entire teaching staff of the Electrical Engineering Department at M'sila University.

Our gratitude goes as well to everyone who offered us help and support during the preparation and writing of this thesis.

Last but not least, we would like to thank all our friends and family members.

Dedications

To those who instilled in us values and principles,

To those whose prayers were the secret to our success,

To our dear parents,

We dedicate this work as a token of love and gratitude for all the efforts and sacrifices you have made in raising and educating us.

To our brothers and sisters,

to our honorable sheikhs and professors,

to our loyal friends,

we dedicate the fruit of this humble effort, hoping to meet your expectations.

Student:

SAOUCHI Louey

Dedications

To those who instilled in us values and principles,

To those whose prayers were the secret to our success,

To our dear parents,

We dedicate this work as a token of love and gratitude for all the efforts and sacrifices you have made in raising and educating us.

To our brothers and sisters,

To our honorable sheikhs and professors,

To our loyal friends,

We dedicate the fruit of this humble effort, hoping to meet your expectations.

Student:

BELABBES Fares

Summary

General Introduction

Chapter I
Modeling of the DFIM

Chapter II
The vector control

Chapter III
Fuzzy - SMC - PI Control

LIST OF FIGURES

Chapter I

Modeling of the DFIM

Chapter II

The vector control

Chapter III

FUZZY - SMC – PI Control

General Introduction

Doubly-fed induction machines (DFIM) have become a cornerstone solution in modern variable-speed drive systems, particularly in medium- and high-power applications such as wind turbines, industrial drives, motor-generator sets, and other renewable energy systems [1]. The machines in question are composed of a stator connected to the power grid and a rotor supplied through a frequency converter. This configuration allows for extended speed control with minimal power electronics, typically around 25 to 30% of the nominal power. This characteristic renders DFIM a more cost-effective solution in comparison to full-power synchronous machines. Furthermore, it offers a significant advantage in terms of reduced energy loss and operational flexibility [2].

Nevertheless, despite their numerous advantages, the dynamic complexity of DFIM poses significant challenges, particularly in maintaining stable and efficient control. The presence of uncertainties, including load variations, system nonlinearities, and electromagnetic disturbances, introduces additional layers of difficulty in achieving precise control. The inherent coupling between the stator and rotor circuits, in conjunction with time-varying operational conditions, renders DFIM control more challenging than that of traditional induction machines [3]. Whilst PI controllers are extensively employed in industrial contexts due to their simplicity and satisfactory performance under nominal conditions, they frequently prove to be inadequate when confronted with parameter variations, external disturbances or rapid changes in load conditions. This phenomenon has been observed to result in a marked decline in system performance, particularly in contexts that necessitate precise operation or encounter frequent variations in operational speed and workload [3].

In response to these limitations, more sophisticated control approaches have been proposed. A notable example is Sliding Mode Control (SMC), which has garnered attention due to its robustness and inherent capacity to preserve system performance in the face of uncertainties and external disturbances. SMC offers the advantage of ensuring that the system reaches a desired trajectory, regardless of variations in system parameters or external disturbances. However, a salient drawback of SMC is the phenomenon of "chattering," which can lead to undesirable high-frequency oscillations that may damage the actuators or reduce system efficiency [4].

In addressing this issue, the integration of fuzzy logic has been demonstrated to be a highly effective strategy for enhancing the overall performance of DFIM. Fuzzy logic controllers offer a flexible approach that adapts in real time to varying system dynamics, thereby providing a smoother control response while mitigating the chattering effect that is often observed in SMC. Enabling dynamic adjustment of control parameters based on the real-time state of the system has been demonstrated to enhance system stability, reduce undesirable oscillations, and improve overall robustness in unpredictable environments [5]. Furthermore, fuzzy logic controllers are particularly well-suited to handling the nonlinearities that are characteristic of DFIM systems, thus rendering them an ideal complement to traditional control methods such as PI and SMC.

In recent years, there has been a notable surge of interest in the integration of multiple control techniques with fuzzy logic as a means to enhance the performance of complex and nonlinear systems. In this context, this thesis proposes a hybrid control strategy that integrates PI control, SMC, and fuzzy logic. This represents a promising avenue for improving the speed control performance of DFIM. This hybrid approach has the

potential to combine the strengths of each individual technique: the simplicity and effectiveness of PI controllers in steady-state conditions, the robustness and disturbance rejection capability of SMC, and the real-time adaptability and flexibility of fuzzy logic. Collectively, these methodologies constitute a comprehensive and efficient solution, capable of enhancing the dynamic response, stability, and efficiency of DFIM, even in the face of complex, real-world operating conditions.

This thesis is divided into three chapters:

In the first chapter, the classical modelling of the doubly fed asynchronous machine in the Park frame linked to the rotating field (d, q) with a view to its control using the state formalism is first recalled, followed by the presentation of the models in the form of a block diagram. Subsequently, an overview of the pulse width modulation control of voltage inverters will be provided.

In the subsequent chapter, the principle of vector control applied to the doubly fed asynchronous machine will be presented, in addition to a concise review of the principle of oriented stator flux vector control. In this type of control, the machine is operated in a manner analogous to that of the separately excited direct current machine.

The objective of the final chapter is to develop a robust nonlinear control system that integrates elements of PI control, sliding mode control and fuzzy logic. The control in question involves the replacement of the regulator applied to the vector control with a regulator based on PI, SMC and fuzzy logic of type 1. Consequently, an intelligent hybrid control strategy will be presented and evaluated by numerous simulations, taking into account parametric uncertainties. This will verify the interest of this approach and allow for comparisons to be made with the results obtained by the vector control.

In conclusion, a general conclusion is provided to summarise the present study and to propose potential avenues for future research.

Chapter I

Modeling of the DFIM

I.1 Introduction:

To achieve an efficient control of a dynamic system, we must have a mathematical model that adequately represents the actual behavior of the system. For the doubly-fed induction machine (DFIM), modeling is an essential phase that requires a thorough understanding of its electromechanical structure, electrical structure (power supply), and mechanical structure (rotating mass, resistant torque, viscous friction). It is therefore evident that this modeling step is a necessary prerequisite for developing control laws. The representation of the mathematical model of the DFIM allows for both the observation and analysis of the various evolutions of its electromechanical quantities and the anticipation of the necessary control adjustments, if needed, to compensate for the different effects that may typically accompany operations such as startup, speed variation.

In this chapter, we will present the classical modeling of the DFIM and its power supply. We will define a mathematical model of the machine by expressing the electrical, magnetic, and mechanical equations governing its operation in the three-phase reference frame (A, B, C). The system's order will then be reduced, and the dependence between the inductance coefficients and the rotor position will be eliminated using the Park transformation.

Next, we will introduce the modeling of the power supply system, starting with the voltage inverter, which is responsible for DC-AC conversion and its sinusoidal PWM (Pulse Width Modulation) control, followed by the grid-side converter (PWM rectifier). A series of simulations using Matlab/Simulink has been verify the performance of the converter-DFIM association under different conditions and validate the obtained model.

I.2 Mathematical Model of the (DFIM)

The doubly-fed asynchronous machine consists of a stator and a rotor, each with three windings distributed 120 degrees apart. Unlike conventional machines, the rotor is connected through slip rings. The machine is typically modeled using the two-axis method, which transforms the three-phase system into a two-phase system, with certain simplifying assumptions applied to ease the mathematical modeling.

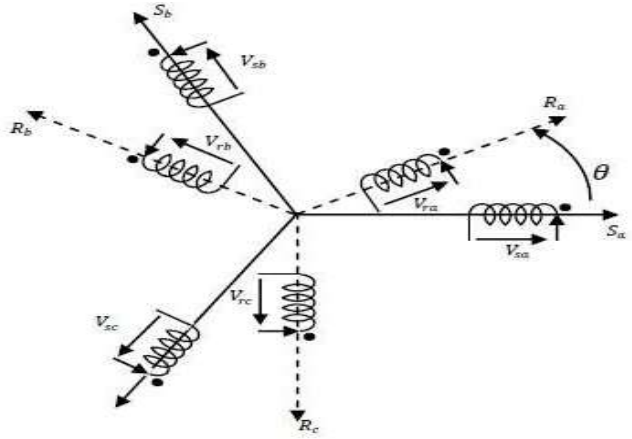

Figure (I.1): Schematic Representation of the (DFIM) in the Three-Phase System.

I.2.1 Electrical Equations

From Figure (I.1), the electrical equations of the doubly-fed asynchronous machine model are written respectively for the stator with the index (s) and the rotor with the index (r) as follows:

For stator winding:

$$\begin{cases} V_{sa} = R_s I_{sa} + \frac{d\varphi_{sa}}{dt} \\ V_{sb} = R_s I_{sb} + \frac{d\varphi_{sb}}{dt} \\ V_{sc} = R_s I_{sc} + \frac{d\varphi_{sc}}{dt} \end{cases} \quad \text{(I.1)}$$

For rotor winding:

$$\begin{cases} V_{ra} = R_r I_{ra} + \frac{d\varphi_{ra}}{dt} \\ V_{rb} = R_r I_{rb} + \frac{d\varphi_{rb}}{dt} \\ V_{rc} = R_r I_{rc} + \frac{d\varphi_{rc}}{dt} \end{cases} \quad \text{(I.2)}$$

Or in matrix forms

$$\begin{bmatrix} V_{sa} \\ V_{sb} \\ V_{sc} \end{bmatrix} = \begin{bmatrix} R_s & 0 & 0 \\ 0 & R_s & 0 \\ 0 & 0 & R_s \end{bmatrix} . \begin{bmatrix} I_{sa} \\ I_{sb} \\ I_{sc} \end{bmatrix} + \frac{d}{dt} \begin{bmatrix} \varphi_{sa} \\ \varphi_{sb} \\ \varphi_{sc} \end{bmatrix} \quad \text{(I.3)}$$

$$\begin{bmatrix} V_{ra} \\ V_{rb} \\ V_{rc} \end{bmatrix} = \begin{bmatrix} R_r & 0 & 0 \\ 0 & R_r & 0 \\ 0 & 0 & R_r \end{bmatrix} . \begin{bmatrix} I_{ra} \\ I_{rb} \\ I_{rc} \end{bmatrix} + \frac{d}{dt} \begin{bmatrix} \varphi_{ra} \\ \varphi_{rb} \\ \varphi_{rc} \end{bmatrix} \quad \text{(I.4)}$$

With:

V,I, and φ are the voltage, current, and flux, respectively.

R_s And R_r are the stator and rotor resistances, respectively.

I.2.2 Magnetic Equations

The hypotheses we previously presented lead to linear relationships between flux and currents.

$$\begin{bmatrix} \varphi_{sa} \\ \varphi_{sb} \\ \varphi_{sc} \end{bmatrix} = \begin{bmatrix} l_s & M_s & M_s & M_1 & M_3 & M_2 \\ M_s & l_s & M_s & M_2 & M_1 & M_3 \\ M_s & M_s & l_s & M_3 & M_2 & M_1 \end{bmatrix} . \begin{bmatrix} I_{sa} \\ I_{sb} \\ I_{sc} \\ I_{ra} \\ I_{rb} \\ I_{rc} \end{bmatrix} \quad \text{(I.5)}$$

$$\begin{bmatrix} \varphi_{ra} \\ \varphi_{rb} \\ \varphi_{rc} \end{bmatrix} = \begin{bmatrix} M_1 & M_2 & M_3 & l_r & M_r & M_r \\ M_3 & M_1 & M_2 & M_r & l_r & M_r \\ M_2 & M_3 & M_1 & M_r & M_r & l_r \end{bmatrix} . \begin{bmatrix} I_{sa} \\ I_{sb} \\ I_{sc} \\ I_{ra} \\ I_{rb} \\ I_{rc} \end{bmatrix} \quad \text{(I.6)}$$

With:

l_s, l_r :Self-inductances of a stator phase and a rotor phase.

M_s, M_r: Mutual inductances between two stator phases and two rotor phases.

M_1,M_2 , M_3:Instantaneous mutual inductances between a stator phase and a rotor phase.

$$\begin{bmatrix} M_1 \\ M_2 \\ M_3 \end{bmatrix} = M_0 \begin{bmatrix} cos(\theta) \\ cos\left(\theta - \frac{2\pi}{3}\right) \\ cos\left(\theta + \frac{2\pi}{3}\right) \end{bmatrix} \quad (I.7)$$

M_0: Maximum mutual inductance between a stator phase and a rotor phase.

The actual flux matrix reveals two sub-matrices of inductances:

$$[\varphi_{sabc}] = [L_s][I_{sabc}] + [M_{sr}][I_{rabc}] \quad (I.8)$$

$$[\varphi_{rabc}] = [M_{rs}][[I_{sabc}]] + [L_r][I_{rabc}] \quad (I.9)$$

With

$$[L_s] = \begin{bmatrix} L_s & M_s & M_s \\ M_s & L_s & M_s \\ M_s & M_s & L_s \end{bmatrix} \quad (I.10)$$

$$[L_r] = \begin{bmatrix} L_r & M_r & M_r \\ M_r & L_r & M_r \\ M_r & M_r & L_r \end{bmatrix} \quad (I.11)$$

$$[M_{sr}] = [M_{rs}]^T = M_0 . \begin{bmatrix} cos(\theta) & cos\left(\theta + \frac{2\pi}{3}\right) & cos\left(\theta - \frac{2\pi}{3}\right) \\ cos\left(\theta - \frac{2\pi}{3}\right) & cos(\theta) & cos\left(\theta + \frac{2\pi}{3}\right) \\ cos\left(\theta + \frac{2\pi}{3}\right) & cos\left(\theta - \frac{2\pi}{3}\right) & cos(\theta) \end{bmatrix} \quad (I.12)$$

I.2.3 Mechanical Equation

The mechanical equation of the machine is given as follows:

$$T_{em} = T_r + f\Omega + j\frac{d\Omega}{dt} \quad (I.13)$$

With:

- T_{em} : Electromagnetic torque of the machine ;
- T_r : Resistive torque ;
- f: Viscous friction coefficient of the Doubly-Fed Induction Machine (MADA);
- Ω : Rotational speed of the MADA shaft;
- j : Inertia of the rotating parts.

The general expression of the electromagnetic torque is given by:

$$T_{em} = \frac{1}{2} P[I]^T \frac{d[L]}{dt} . [I] \quad (I.14)$$

With:

$$[I] = [I_{sa} \;\; I_{sb} \; I_{sc} \;\; I_{ra} \;\; I_{rb} \;\; I_{rc}]^T = \begin{bmatrix} [I_s] \\ [I_r] \end{bmatrix} \quad (I.15)$$

[L]: Total Inductance Matrix

$$[\mathrm{L}] = \begin{bmatrix} [L_s] & [M_{sr}] \\ [M_{rs}] & [L_r] \end{bmatrix} \quad (I.16)$$

P : The number of pole pairs;

The matrices $[L_s]$ and $[L_r]$ contain only constant terms when the angle θ varies, which simplifies the expression of the torque.

$$T_{em} = \text{p}.[I_s]^T \frac{d}{dt}[[M_{sr}].[I_r]] \quad \text{(I.17)}$$

I.3 Park Transformation

The model of the Doubly-Fed Induction Machine (DFIM) in the (A, B, C) reference frame is highly complex and leads to differential equations with variable coefficients. The purpose of matrix transformations is to simplify it by reducing the system's order and eliminating its dependence on the rotor position. This results in a model characterized by a system of equations with constant coefficients [5].

The Park transformation is a mathematical tool that enables the conversion from a three-phase alternating system (a, b, c reference frame) to a two-phase system (d, q reference frame).

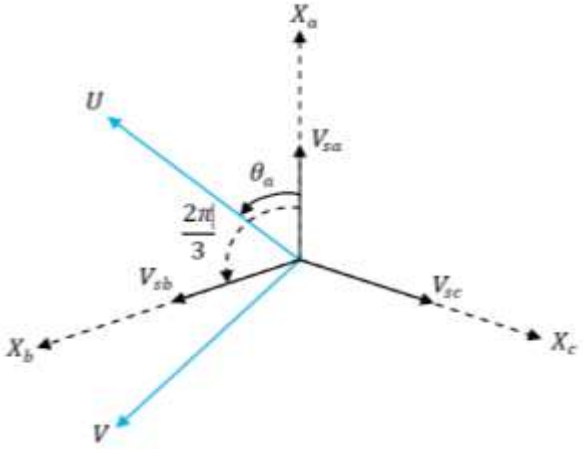

Figure (I.2) : Conversion from a Three-Phase System to a Two-Phase System and Vice Versa.

θ_a: Represents the instantaneous angle between the phase of the X_a axis and the U axis.

$\omega_a = \frac{d\theta_a}{dt}$ Angular velocity of the rotating two-phase reference frame relative to the three-phase reference frame.

According to Figure (I.1), the projection of the vector V_{sa}, V_{sb} V_{sc} onto the two-phase axis gives us

$$\begin{cases} \text{V}_{\text{su}} = \sqrt{\frac{2}{3}}[\text{V}_{\text{sa}}.\cos\theta_a + \text{V}_{\text{sb}}.\cos(\theta_a - \frac{2\pi}{3}) + \text{V}_{\text{sc}}.\cos(\theta_a - \frac{4\pi}{3})] \\ \text{V}_{\text{su}} = -\sqrt{\frac{2}{3}}[\text{V}_{\text{sa}}.\sin\theta_a + \text{V}_{\text{sb}}.\sin(\theta_a - \frac{2\pi}{3}) + \text{V}_{\text{sc}}.\sin(\theta_a - \frac{4\pi}{3})] \end{cases} \quad \text{(I.18)}$$

The term $\sqrt{\frac{2}{3}}$ expresses the conversion from the three-phase system to the two-phase system while preserving power.

The homopolar component V_{so} is added to equation (I.18) to balance the transformation.

$$V_{so} = \frac{1}{3}(V_{sa} + V_{sb} + V_{sc}) \quad \text{(I.19)}$$

The homopolar component V_{so} is zero for balanced three-phase systems.

From equations (I.18) and (I.19), we obtain:

$$\begin{bmatrix} V_{su} \\ V_{sv} \\ V_{so} \end{bmatrix} = [P(\theta_a)].\begin{bmatrix} V_{sa} \\ V_{sb} \\ V_{sc} \end{bmatrix} \quad \text{(I.20)}$$

The conversion from the three-phase system to the two-phase system is achieved using the transformation matrix$[P(\theta_a)]$:

$$[P(\theta_a)] = \sqrt{\frac{2}{3}}\begin{bmatrix} cos(\theta_a) & -(sin\,\theta_a) & \frac{1}{\sqrt{2}} \\ cos(\theta_a - \frac{2\pi}{3}) & -(sin\,\theta_a - \frac{2\pi}{3}) & \frac{1}{\sqrt{2}} \\ cos(\theta_a - \frac{4\pi}{3}) & -(sin\,\theta_a - \frac{4\pi}{3}) & \frac{1}{\sqrt{2}} \end{bmatrix} \quad \text{(I.21)}$$

$$\begin{bmatrix} V_{su} \\ V_{sv} \\ V_{so} \end{bmatrix} = [P(\theta_a)]^{-1}.\begin{bmatrix} V_{sa} \\ V_{sb} \\ V_{sc} \end{bmatrix} \quad \text{(I.22)}$$

$$[P(\theta_a)]^{-1} = \sqrt{\frac{2}{3}}\begin{bmatrix} cos(\theta_a) & -(sin\,\theta_a) & \frac{1}{\sqrt{2}} \\ cos(\theta_a - \frac{2\pi}{3}) & -(sin\,\theta_a - \frac{2\pi}{3}) & \frac{1}{\sqrt{2}} \\ cos(\theta_a - \frac{4\pi}{3}) & -(sin\,\theta_a - \frac{4\pi}{3}) & \frac{1}{\sqrt{2}} \end{bmatrix} \quad \text{(I.23)}$$

I.3.1 Electrical Equations

The Park transformation involves applying a variable change to currents, voltages, and fluxes by incorporating the angle between the winding axis and the (u, v) axis.

Equations (I.3) and (I.4) then lead to the following system after the calculations detailed in Appendix [A]:

$$\begin{bmatrix} V_{su} \\ V_{sv} \end{bmatrix} = \begin{bmatrix} R_s & 0 \\ 0 & R_s \end{bmatrix}.\begin{bmatrix} I_{su} \\ I_{sv} \end{bmatrix} + \frac{d}{dt}\begin{bmatrix} \varphi_{su} \\ \varphi_{sv} \end{bmatrix} + \begin{bmatrix} 0 & -\omega_a \\ \omega_a & 0 \end{bmatrix}.\begin{bmatrix} \varphi_{su} \\ \varphi_{sv} \end{bmatrix} \quad \text{(I.24)}$$

$$\begin{bmatrix} V_{ru} \\ V_{rv} \end{bmatrix} = \begin{bmatrix} R_r & 0 \\ 0 & R_r \end{bmatrix}.\begin{bmatrix} I_{ru} \\ I_{rv} \end{bmatrix} + \frac{d}{dt}\begin{bmatrix} \varphi_{ru} \\ \varphi_{rv} \end{bmatrix} + \begin{bmatrix} 0 & -(\omega_a - \omega) \\ (\omega_a - \omega) & 0 \end{bmatrix}.\begin{bmatrix} \varphi_{ru} \\ \varphi_{rv} \end{bmatrix} \quad \text{(I.25)}$$

I.3.2 Magnetic Equations

Similarly, from equations (II.5) and (II.6), the calculations detailed in [HER], we obtain:

$$\begin{bmatrix} \varphi_{su} \\ \varphi_{ru} \end{bmatrix} = \begin{bmatrix} L_s & M \\ M & L_r \end{bmatrix}.\begin{bmatrix} I_{su} \\ I_{ru} \end{bmatrix} \quad \text{(I.26)}$$

$$\begin{bmatrix} \varphi_{sv} \\ \varphi_{rv} \end{bmatrix} = \begin{bmatrix} L_s & M \\ M & L_r \end{bmatrix}.\begin{bmatrix} I_{sv} \\ I_{rv} \end{bmatrix} \quad \text{(I.27)}$$

$L_s = I_s - M$: Cyclic self-inductance of the stator.

$L_r = I_r - M$: Cyclic self-inductance of the rotor.

$M = \frac{3}{2} M_0$: Cyclic mutual inductance between the stator and rotor.

I.3.3 Electromagnetic Equation

The equation of the electromagnetic torque using the Park transformation is expressed by four formulas depending on the choice of state variables (stator/rotor flux and stator/rotor current).

T_{em}=P $[\varphi_{su} I_{sv} - \varphi_{sv} I_{su}]$ (I.28)

T_{em}=P $[\varphi_{ru} I_{rv} - \varphi_{rv} I_{ru}]$ (I.29)

$T_{em} = \frac{PM}{Ls} = [\varphi_{su} I_{rv} - \varphi_{sv} I_{ru}]$ (I.30)

T_{em}=$\frac{PM}{Lr}$ $[\varphi_{ru} I_{sv} - \varphi_{rv} I_{su}]$ (I.31)

P: Number of pole pairs

I.3.4 reference (d,q)

There are different possibilities for choosing the orientation of the (u,) axis system, which generally depend on the application objectives. The choice is practically reduced to three orthogonal reference frames, as shown in Figure (I.2):

- Reference frame with axes α: A two-phase system with orthogonal axes where$\theta_a = 0$.
- Reference frame with axes d,: A two-phase system with orthogonal axes where $\theta_a = \theta_s$
- Reference frame with axes x: A two-phase system with orthogonal axes where$\theta_a = \theta_r$.

The angle θa represents an arbitrary observation position that can be chosen in three different ways.

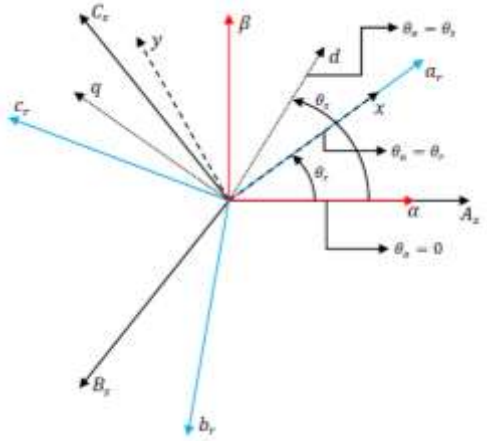

Figure (I.3): Definition of the Actual Axes of the MADA in Relation to the Different Reference Frames

$\omega_s = \frac{d\theta_s}{dt}$: Electrical rotational speed of the reference frame linked to the rotating field.

$\omega_r = \frac{d\theta_r}{dt}$: Electrical slip speed.

$\omega = \frac{d\theta}{dt}$: Electrical rotational speed of the rotor relative to the stator**.**

It is defined by the following conditions:

$$\theta_a = 0 \Leftrightarrow \begin{cases} u = d \\ v = q \end{cases}$$

$$\frac{d\theta_a}{dt} = \omega_a = \omega_s, \qquad with: \ \omega_s - \omega = \omega_r$$

The electrical equations take the following form:

$$\begin{bmatrix} V_{sd} \\ V_{sq} \end{bmatrix} = \begin{bmatrix} R_s & 0 \\ 0 & R_s \end{bmatrix} \cdot \begin{bmatrix} I_{sd} \\ I_{sq} \end{bmatrix} + \frac{d}{dt} \begin{bmatrix} \varphi_{sd} \\ \varphi_{sq} \end{bmatrix} + \begin{bmatrix} 0 & -\omega_r \\ \omega_r & 0 \end{bmatrix} \cdot \begin{bmatrix} \varphi_{sd} \\ \varphi_{sq} \end{bmatrix} \quad (I.32)$$

$$\begin{bmatrix} V_{rd} \\ V_{rq} \end{bmatrix} = \begin{bmatrix} R_r & 0 \\ 0 & R_r \end{bmatrix} \cdot \begin{bmatrix} I_{rd} \\ I_{rq} \end{bmatrix} + \frac{d}{dt} \begin{bmatrix} \varphi_{rd} \\ \varphi_{rq} \end{bmatrix} + \begin{bmatrix} 0 & -\omega_r \\ \omega_r & 0 \end{bmatrix} \cdot \begin{bmatrix} \varphi_{rd} \\ \varphi_{rq} \end{bmatrix} \quad \text{(I.33)}$$

The flux expressions, based on equations (I.26) and (I.27), are given by:

$$\begin{cases} \varphi_{sd} = L_s I_{sd} + M I_{rd} & \text{(a)} \\ \varphi_{sq} = L_s I_{sq} + M I_{rq} & \text{(b)} \\ \varphi_{rd} = L_r I_{rd} + M I_{sd} & \text{(c)} \\ \varphi_{rq} = L_r I_{rd} + M I_{sq} & \text{(d)} \end{cases} \quad \text{(I.34)}$$

This reference frame is often used in the study of variable-frequency asynchronous motor control. It is particularly utilized in the control of electrical machines in closed-loop systems, where the controlled quantities must necessarily be in a continuous form.

I.4 State Equation Formulation:

The model of the doubly-fed asynchronous machine (DFIM) supplied by voltage includes stator voltages (V_{sd}) and rotor voltages (V_{sd}, V_{sq}), with the resistant torque C_r as a disturbance. The system can be described using multiple state variables. However, our study will be limited to a specific case represented by the stator flux components and the rotor current components ($\varphi_{sd}\ \varphi_{sq}\ I_{rd}\quad I_{rq}$)

After rearranging equations (I.36), (I.37), and (I.38), we obtain:

$$\begin{cases} V_{sd} = R_s I_{sd} + L_s + L_s \frac{dI_{sd}}{dt} + M \frac{dI_{rd}}{dt} - \omega_s L_s L_{sq} - \omega_s M I_{rq} \\ V_{sq} = R_s I_{sq} + L_s + L_s \frac{dI_{sq}}{dt} + M \frac{dI_{rq}}{dt} - \omega_s L_s L_{sd} + \omega_s M I_{rd} \\ V_{rd} = R_r I_{rd} + L_r + L_r \frac{dI_{rd}}{dt} + M \frac{dI_{sd}}{dt} - \omega L_r L_{rq} - \omega M I_{sq} \\ V_{rq} = R_r I_{rq} + L_r + L_r \frac{dI_{rq}}{dt} + M \frac{dI_{sq}}{dt} - \omega L_r L_{rd} - \omega M I_{sd} \end{cases} \quad \text{(I.35)}$$

Moreover, the equations representing the mechanical motion are given by:

$$T_{em} = P \frac{M}{L_s} (\varphi_{sq} I_{rd} - \varphi_{sd} I_{rq}) \quad \text{(I.36)}$$

$$T_{em} - T_r = j \frac{d\Omega}{dt}. + F\omega \quad \text{(I.37)}$$

This system can be written in state-space form:

$$[\dot{X}] = [A].[X] + [B].[U] \quad \text{(I.38)}$$

Withe:

$[X] = [\varphi_{sd}\ \varphi_{sq}\ I_{rd}\quad I_{rq}]^T$: State vector

$[U] = [V_{sd}\ \ V_{sq}\quad V_{rd}\ V_{rq}]^T$: Control vector

A: State evolution matrix of the system

B: Control matrix of the system.

Such that:

$$[A]=\begin{bmatrix} \frac{-1}{T_s} & \omega_s & \frac{M}{T_s} & 0 \\ -\omega_s & \frac{-1}{T_s} & 0 & \frac{M}{T_s} \\ \alpha & -\beta\omega_s & -\delta & (\omega_s-\omega) \\ \beta\omega & \alpha & -(\omega_s-\omega) & -\delta \end{bmatrix}, \qquad [B]=\begin{bmatrix} 1 & 0 & 0 & 0 \\ 0 & 1 & 0 & 0 \\ -\beta & 0 & \frac{1}{\sigma Lr} & 0 \\ 0 & -\beta & 0 & \frac{1}{\sigma Lr} \end{bmatrix}$$

α, β, and δ\deltaδ are constants defined as follows:

$\alpha = \frac{M}{\sigma TsLsLr}$, $\beta=\frac{M}{\sigma LsLr}$ and$\delta = \frac{1}{\sigma}.(\frac{1}{Tr}+\frac{M^2}{TsLsLr})$

Where:

$T_{s=}\frac{Ls}{Lr}$ And $T_r = \frac{Lr}{Rr}$

To facilitate the simulation, the matrix [A] is decomposed as follows:

$$[A] = [A1] + \omega_s[A2] + \omega[A3] \qquad (I.39)$$

"Such that:

$$[A1]=\begin{bmatrix} \frac{-1}{Ts} & 0 & \frac{M}{TS} & 0 \\ 0 & \frac{-1}{Ts} & 0 & \frac{M}{TS} \\ \alpha & 0 & -\delta & 0 \\ 0 & \alpha & 0 & -\delta \end{bmatrix},[A2]=\begin{bmatrix} 0 & 1 & 0 & 0 \\ -1 & 0 & 0 & 0 \\ 0 & 0 & 0 & 1 \\ 0 & 0 & -1 & 0 \end{bmatrix},[A3]=\begin{bmatrix} 0 & 0 & 0 & 0 \\ -0 & 0 & 0 & 0 \\ 0 & -\beta & 0 & -1 \\ \beta & 0 & 1 & 0 \end{bmatrix},$$

I.5 Simulation Results

The state-space representation of the doubly-fed induction machine model allows for its simulation. The objective of this study, presented in this section, is to develop a block diagram, as illustrated in Figure (I.4), from which the DFIM is directly supplied by the three-phase network [220/380V, 50Hz]. The parameters of the doubly-fed induction machine used in this work are provided in Appendix [A].

We perform a no-load start-up (Cr = 0 N·m), and at the moment (t = 2 s), a load is applied (Cr = 15 N·m). The simulation results are presented in Figure (I.4).

In this case, we observe a decrease in speed that stabilizes at a value of 151 rad/s, indicating an increase in the machine's slip. The electromagnetic torque reaches the value that compensates for the applied resistant torque, showing good tracking of the reference value (15 N·m), which offsets the effect of the load and friction.

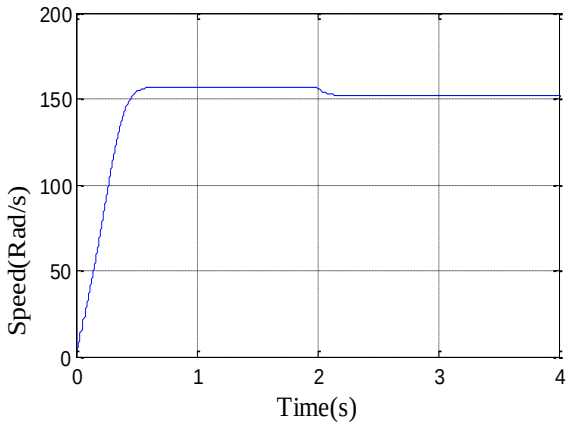

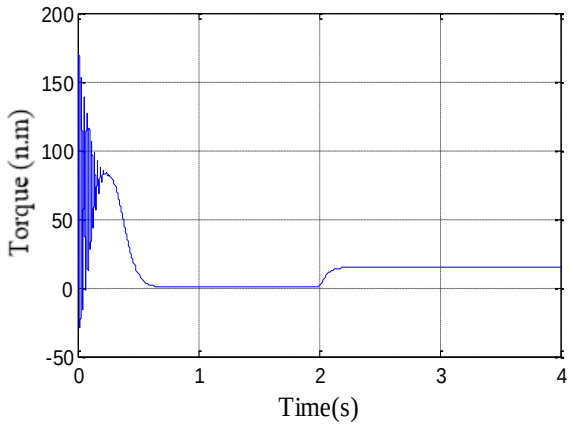

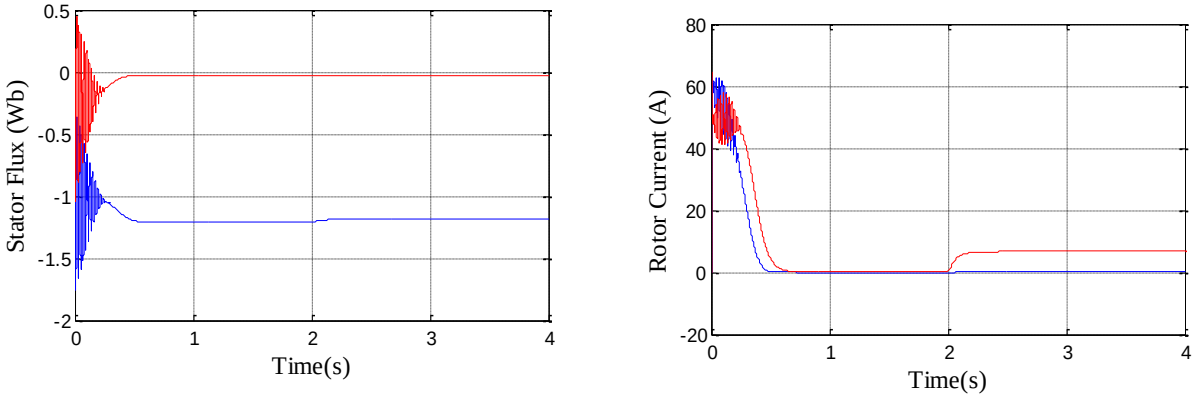

Figure (I.4): Simulation Results of the DFIM

The stator fluxes maintain their shapes with a slight decrease in their magnitudes. The rotor currents show an increase in amplitude due to the increased load. It is also observed that the flux varies with the variation of the load, demonstrating a strong coupling between torque and flux.

I.6 System Power Supply Modeling:

For variable speed drives of asynchronous motors, voltage inverters are commonly used. When powered by the mains, the entire electric drive system includes:

- An input rectifier,
- A low-pass filter with a large-capacity capacitor that makes the ripple of the voltage U at the inverter input negligible,
- A voltage inverter,
- The asynchronous motor

I.6.1 The Structure of the Selected Power Supply Chain:

Figure I.5 illustrates the detailed diagram of the converters supplying power to the machine.

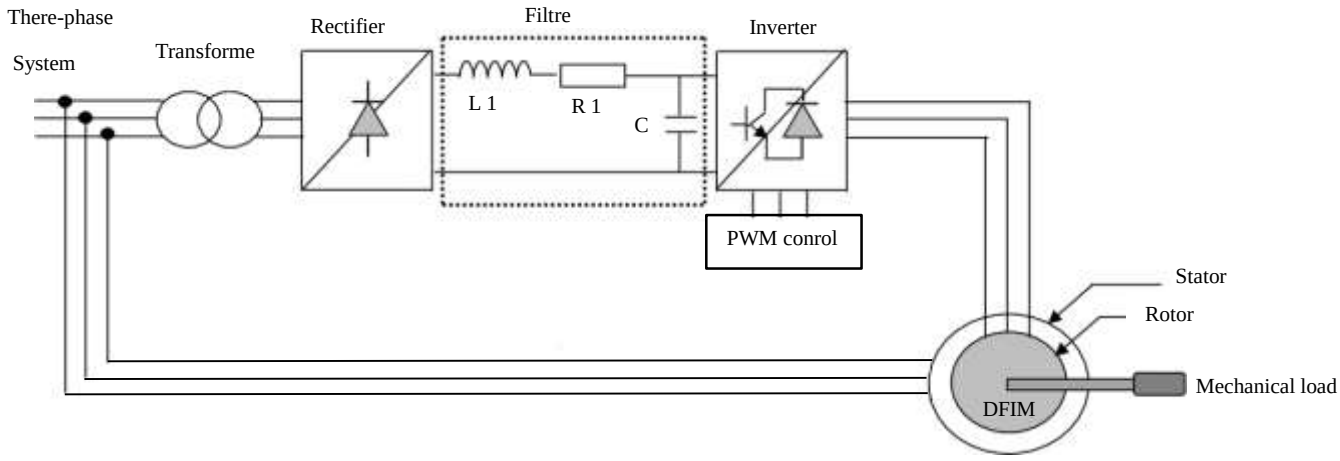

Figure (I.5): Proposed Block Diagram for Supplying Power to the Machine

I.6.2 Rectifier Modeling:

The rectifier is a static converter capable of transforming energy from an AC source into a DC source. There are several configurations, and the choice depends on the desired performance.

In our work, we focus only on the three-phase, uncontrolled full-wave rectifier, whose components are diodes. The rectifier is supplied by a three-phase electrical network with a balanced voltage system**.**

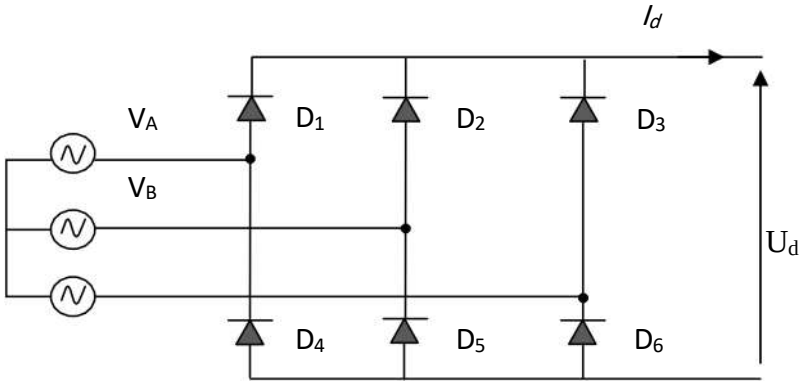

Figure (I.6): Representation of the Three-Phase Diode Rectifier

Diodes D1, D2, and D3 have a common cathode and ensure the forward path of the currentI_d.

Diodes D4, D5, and D6 have a common anode and ensure the return path of the currentI_d.

It is assumed that the three-phase supply source is balanced, with constant voltage amplitude and frequency. Voltage drops due to commutation overlap and losses in the diodes are also neglected. The rectifier is therefore supplied by the following three-phase system:

$$\begin{cases} V_A = V_m \sin(\omega t) \\ V_B = V_m \sin(\omega t - \frac{2\pi}{3}) \\ V_C = V_m \sin(\omega t - \frac{4\pi}{3}) \end{cases} \quad \text{(I.40)}$$

The voltage at the output of the rectifier is given by:

$$U_{red}(t) = max[V_A(t), V_B(t), V_C(t)] \min[V_A(t), V_B(t), V_C(t)] \quad \text{(I.41)}$$

And its average value is given by:

$$\overline{U}_{red} = \frac{3\sqrt{3}}{\pi V_m} \quad \text{(I.42)}$$

Its ripple factor is given by:

$$K\% = \frac{U_d max - U_d min}{2\overline{U}_d}$$

I.6. 2Filter Modeling

To minimize the ripple of the rectified voltage at the output of the rectifier, a low-pass RLC filter is used .The basic schematic of this filter is shown in the figure below

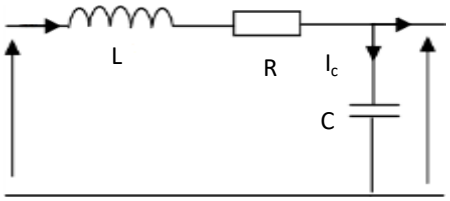

Figure (I.7): Low-Pass RLC Filter

The capacitor allows a nearly constant voltage at the inverter input and absorbs the negative current returned by the load. The inductor helps to make the current nearly constant

The equations of the filter are given by:

$$U_d(t) = L\frac{dI_d}{dt} + RdI_d + \mathrm{U}_{dc}(\mathrm{t}) \quad \text{(I.43)}$$

$$\frac{\mathrm{dU_{dc}}}{\mathrm{dt}} = \frac{1}{\mathrm{c}}(\mathrm{I_d(t)} - \mathrm{I(t)}) \quad \text{(I.44)}$$

The transfer function of the filter is given by:

$$\frac{U_{dc}}{U_d(t)} = \frac{U_{filtree}}{U_{\mathrm{Rectifier}}} = \frac{1}{L.C.S^2 + R.C.s + 1} \quad \text{(I.45)}$$

It is a second-order filter whose cutoff angular frequency is:

$$\omega_c = \frac{1}{\sqrt{L.C}} = 2\pi.f_c$$

f_c: is the cutoff frequency of the filter

I.7 Modeling of the Voltage Inverter:

Inverters are used in various power electronics applications, particularly in controlling the speed of AC motors. An inverter is a static converter that transforms DC voltage into AC voltage by switching the input voltage and applying it to the load alternately in both directions. The control of the inverter switches plays a crucial role, as it determines the shape of the output voltage.

In recent years, inverters have seen significant development thanks to:

- Advances in fully controllable semiconductor components, which are now more powerful, robust, and faster.
- The widespread adoption of Pulse Width Modulation (PWM) techniques.

In this section, we will model a two-level voltage inverter, as well as the PWM control techniques: sinusoidal-triangular and space vector modulation.

I.7.1 Principle of the Two-Level Voltage Inverter:

The three-phase two-level inverter consists of a DC voltage source and six electronic switches arranged in a bridge configuration. The DC voltage is usually obtained from a three-phase diode rectifier followed by a filter. This type of inverter is widely used in Pulse Width Modulation (PWM) techniques to supply balanced three-phase loads with variable voltage and frequency.

Each of the three line-to-line output voltages is a bistable waveform that alternates between +E and -E, and they are phase-shifted by 120 degrees ($2\pi/3$ radians) relative to each other.

To obtain AC voltage from a DC source, the voltage is switched and applied to the load alternately in both directions. When powered by an ideal DC source, the inverter produces an AC output in the form of two-level rectangular pulses, with the output frequency determined by the switching control system.

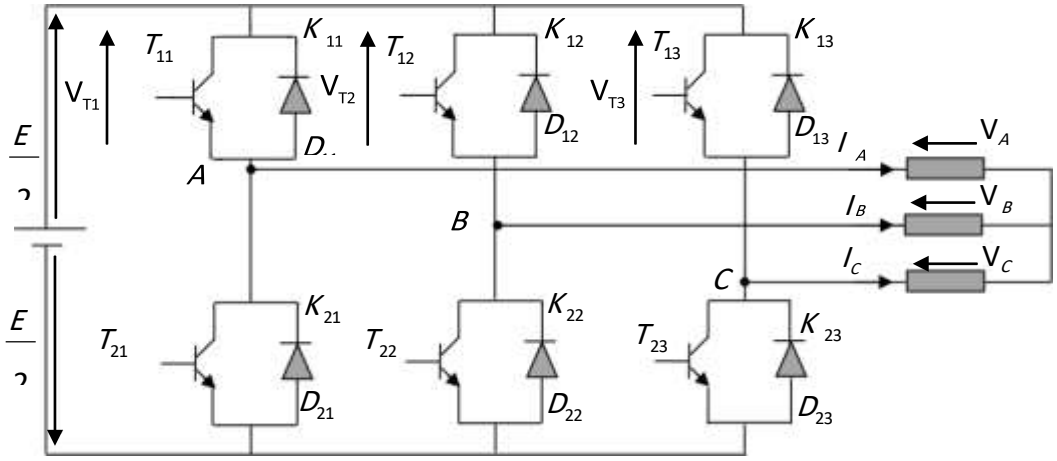

Figure (I.8): Three-Phase Two-Level Voltage Inverte

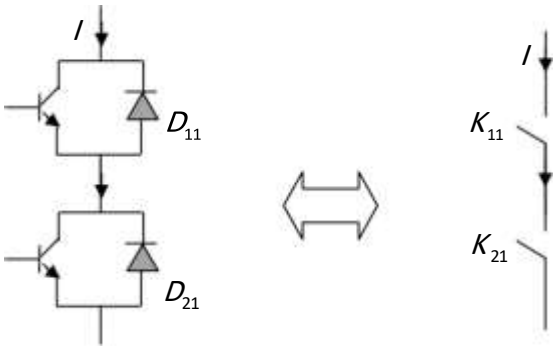

Figure (I.9): Representation of a GTO (Gate Turn-Off Thyristor)

The modeling of the inverter is carried out under the following assumptions:

- The switches are assumed to be ideal (perfect).
- The source in each branch provides a non-zero current, either positive or negative.
- The output voltages at the inverter terminals are referenced with respect to the virtual point "0" at the inverter output**.**

To avoid short-circuiting the DC voltage source, the switching signals within the same inverter leg must be complementary (i.e, the upper and lower switches should not conduct simultaneously).

For simplicity, the load is assumed to be connected in a star configuration without a neutral, although a delta connection is also possible. This setup eliminates third-order harmonics and their multiples, resulting in a balanced three-phase voltage system that contains only odd harmonics not divisible by three.

To generate AC voltage from DC, the input voltage is switched and alternately applied to the load in both directions. When powered by an ideal voltage source, the inverter produces an AC output composed of rectangular pulses, with the operating frequency determined by the switching control. Knowing that we are in a balanced regime $V_{an} + V_{bn} + V_{cn} = 0$ we can write:

$$\begin{cases} V_{an} = V_{ao} + V_{on} \\ V_{bn} = V_{bo} + V_{on} \\ V_{cn} = V_{co} + V_{on} \end{cases} \quad \text{(I.46)}$$

By summing the equations of system (I.46), we obtain:

$$V_{an} + V_{bn} + V_{cn} = V_{ao} + V_{bo} + V_{co} + 3V_{on} = 0 \quad \text{(I.47)}$$

Where:

$$V_{ao} + V_{bo} + V_{co} = -3V_{on} \quad \text{(I.48)}$$

Therefore:

$$V_{on} = \frac{-1}{3} V_{ao} + V_{bo} + V_{co} \quad \text{(I.49)}$$

By substituting equation (I.46) into system (I.49), we then obtain:

$$\begin{bmatrix} V_{an} \\ V_{bn} \\ V_{cn} \end{bmatrix} = \frac{1}{3} \begin{bmatrix} 2 & -1 & -1 \\ -1 & 2 & -1 \\ -1 & -1 & 2 \end{bmatrix} \quad \text{(I.50)}$$

With:

$$\begin{cases} V_{an} = \frac{E}{2} S_1 \\ V_{bn} = \frac{E}{2} S_2 \\ V_{cn} = \frac{E}{2} S_3 \end{cases} \quad \text{(I.51)}$$

Such that:

$$\begin{cases} S_1 = 1 \; if \;\; K_{11} is \; closed, then \; S_1 = +1; otherwise, S_1 = -1, which \; menas \; K_{11} \; is \; open \\ S_2 = 1 \; if \;\; K_{12} is \; closed, then \; S_2 = +1; otherwise, S_2 = -1, which \; menas \; K_{12} \; is \; open \\ S_3 = 1 \; if \;\; K_{13} is \; closed, then \; S_3 = +1; otherwise, S_3 = -1, which \; menas \; K_{13} \; is \; open \end{cases}$$

By substituting equation (I.51) into equation (I.50), we obtain the following system:

$$\begin{bmatrix} V_{an} \\ V_{bn} \\ V_{cn} \end{bmatrix} = \frac{E}{6} \begin{bmatrix} 2 & -1 & -1 \\ -1 & 2 & -1 \\ -1 & -1 & 2 \end{bmatrix} \begin{bmatrix} S_1 \\ S_2 \\ S_3 \end{bmatrix} \quad \text{(I.52)}$$

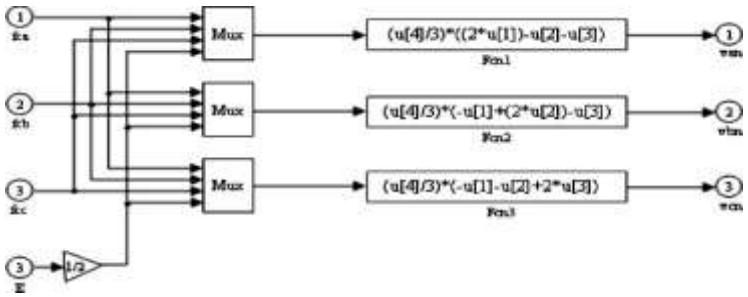

Figure (I.10): Simulink model of the three-phase inverter.

I.7.2 Modeling of Pulse Width Modulation (PWM) Control:

The triangular-sinusoidal modulation, also known as intersected pulse width modulation, is based on comparing:

- A low-frequency modulating signal, usually a sinusoidal reference voltage,
- With a high-frequency carrier wave, generally triangular.

The result of this comparison is used to control the switching (ON/OFF) of the power circuit switches [7].

When the reference is sinusoidal, two key parameters characterize this modulation [7]:

- The modulation index, which defines the ratio between the carrier frequency f_b and the reference frequency f_{ref} of the reference $m = \frac{f_b}{f_{ref}}$
- The modulation ratio rrr (also known as the voltage control coefficient or duty cycle) defines the ratio between the amplitude of the modulating signal V_b and the peak value of the carrier signal V_{ref} of the carrier $r = \frac{v_b}{v_{ref}}$

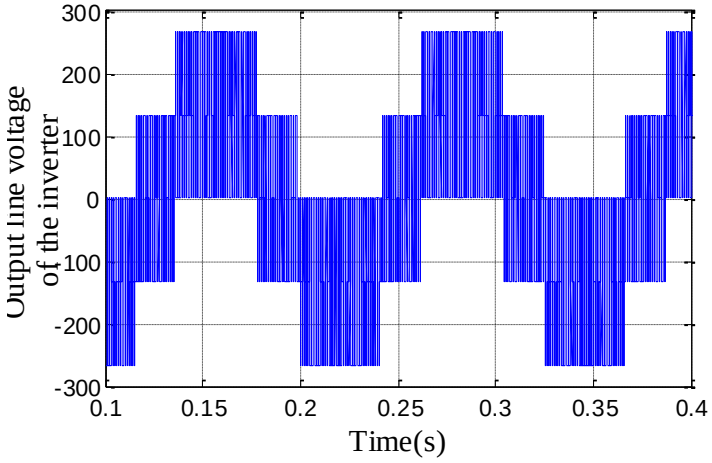

Figure (I.11): Principle of Sinusoidal PWM (Sinus-Triangle Modulation)

(Output line-to-line voltage of the inverter (V))

The carrier is a triangular signal characterized by its frequency f_b and its peak value v_b

The equation of the carrier is defined over its period [0, tp] as follows:

$$\begin{cases} x_1(t) = v_b(-1 + 4\frac{t}{T_p} \\ x_2(t) = v_b(3 - 4\frac{t}{T_p} \end{cases} \quad \text{If} \quad \begin{matrix} \mathrm{t} \in \left[0; \frac{T_p}{2}\right] \\ t \in \left[\frac{T_P}{2}; T_P\right] \end{matrix} \tag{I.53}$$

The reference is a sinusoidal signal with amplitude $V_r$and frequencyf_r.The three sinusoidal reference voltages are given by:

$$\begin{cases} V_{rA(t)=V_r\, sin2\pi f_r t} \\ V_{rB(t)=V_r\, (sin2\pi f_r t - \frac{2\pi}{3})} \\ V_{rC(t)=V_r\, (sin2\pi f_r t + \frac{2\pi}{3})} \end{cases} \tag{I.54}$$

The sinusoidal-triangular PWM control uses the comparison between the carrier and the three components of the reference voltage to calculate the switching statesS_1, S_2 and $S_3$of the inverter switches.

These states are given by the following equation (I.52)

$$S_{123} = \begin{cases} 1\ if\ (V_{r_{ABC}} - x(t)) \geq 0 \\ -1\ if\ (V_{r_{ABC}} - x(t)) \geq 0 \end{cases}$$

It is noted that PWM (Pulse Width Modulation) allows a significant reduction of current harmonics by increasing the switching frequency. It also shifts the voltage harmonics to higher frequencies, which facilitates filtering. Additionally, it allows control over the fundamental component of the desired output voltage

I.7. 3Simulation of the DFIM Coupled with a PWM

The results obtained are summarized in the following figure :

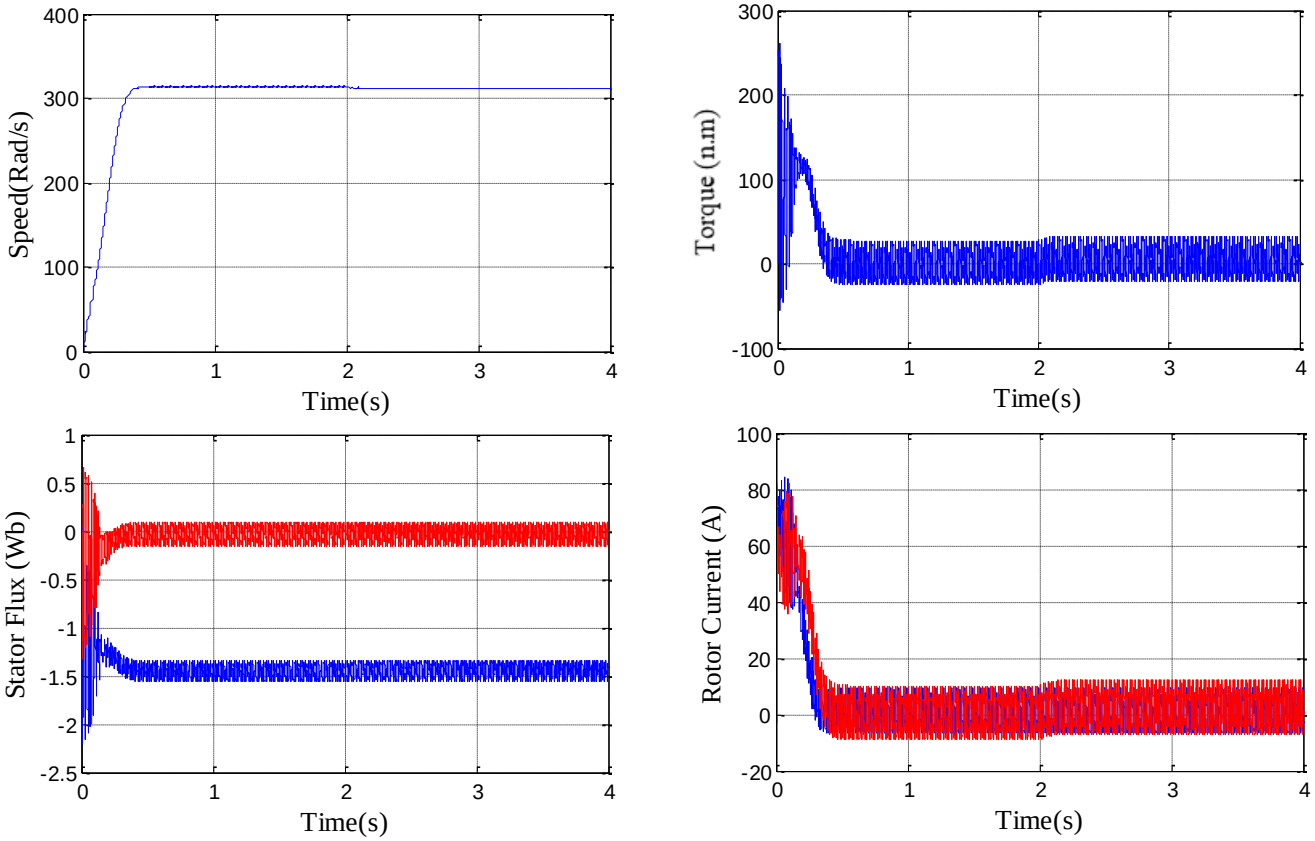

Figure (I.12): Simulation Results for DFIM with PWM

I.7.3.1 Interpretation of the Results:

The stator fluxes maintain their sinusoidal shape with slight amplitude variations, indicating good magnetic stability. The rotor currents exhibit a significant peak during startup, then decrease and stabilize after the load is applied, highlighting the system's ability to handle dynamic changes. These results confirm a strong coupling between torque and flux, and demonstrate the effectiveness of using PWM in reducing harmonics and improving waveform quality, as well as the role of the anodizer in enhancing torque control.

These results indicate stable and efficient system performance, showing good control of torque and flux, along with a clear improvement in the electrical signal quality thanks to the PWM technique.

I.8 Conclusion

In this chapter, we introduced certain simplifying assumptions that must be respected in this work and the Park transformation, which allowed us to derive the mathematical model of the doubly-

fed induction machine (DFIM) linked to the rotating field. During this modeling, we focused on developing a model aimed at the control of the machine.

The simulation of the DFIM and its power supply, performed using MATLAB/SIMULINK, yields open-loop results without any control. However, an increase in load leads to a decrease in speed.

Subsequently, we modeled the inverter that powers the rotor of the DFIM, enabling the application of controls to regulate the power generated by the stator of the machine. Finally, we modeled the power supply of the inverter, which is a three-phase rectifier, and its control to subsequently regulate the DC bus and maintain it at a constant value, with the goal of improving the power factor on the grid side.

However, the machine alone does not always meet the requirements of variable-speed drive systems. It must be coupled with an external controller, which will be discussed in the next chapter, where we will apply vector control to achieve a dynamic behavior similar to that of a DC machine.

Chapter II

The Vector Control Of DFIM

II.1 Introduction

The vector control command was introduced a long time ago; however, it could only be implemented and used effectively with advancements in microelectronics [8]. The basic idea behind this control is to make the behavior of the asynchronous machine identical to that of a separately excited DC machine, where there is a natural decoupling between the flux (the excitation current) and the torque (the armature current) [9].

Vector control with flux orientation presents an attractive solution for achieving better performance in variable speed applications, both in generator and motor operation for the case of the asynchronous machine [1-2]. Today, thanks to this technique and the development of digital systems, many DC drives are being replaced by AC machines, allowing for better speed control in terms of both speed and accuracy [10].

II.2 Principle of Vector Control

Vector control allows the induction machine to operate in a manner similar to a direct current machine, where the electromagnetic torque is proportional to two independent quantities (the flux and the armature current). The control of the induction machine requires the control of torque, speed, or even position. However, the formula for electromagnetic torque is complex. It does not resemble that of a direct current machine, where the decoupling between flux and torque is natural, making its control easier. The magnetomotive force of the armature creates a right angle with the axis of the flux, regardless of the rotational speed. Therefore, the torque is proportional to the product of the flux and the armature current. If the machine is separately excited, and the flux is kept constant, the torque is directly proportional to the armature current, resulting in good dynamic performance. Since the torque can be controlled as quickly as the armature current. On the other hand, in an induction machine, the angle between the rotating field of the stator and that of the rotor varies with the load (different from 90°), resulting in complex interactions and oscillatory dynamic responses [10].

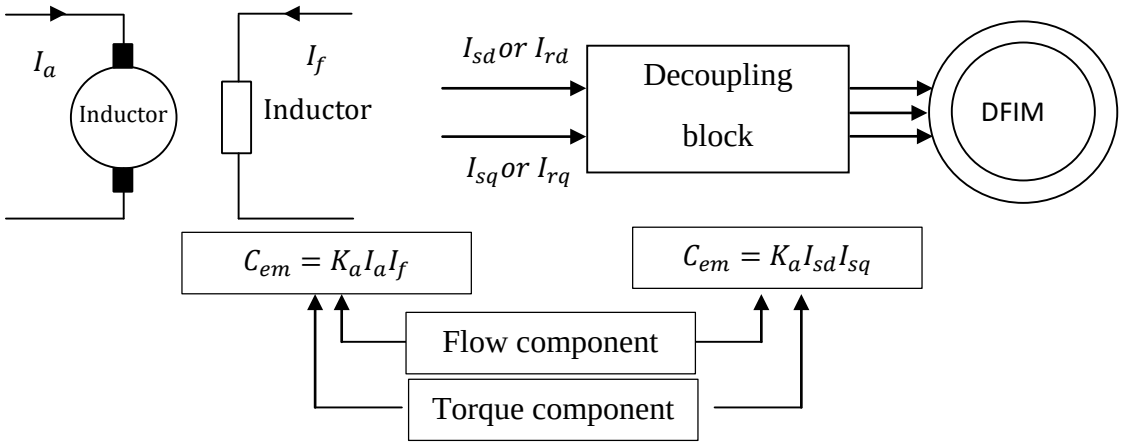

Figure (II.1): Analogy between the vector control of an induction motor (MADA) and the control of a DC motor (MCC).

II.3 Variants of Vector Control

The field-oriented control applied to electric motors is used to achieve the desired operating mode by optimally positioning the current vectors and the resulting flux vectors. Numerous variants of this control principle have been presented in the literature, which can be classified [11]:

- **According to the energy source:**
  - Voltage Source Inverter (VSI) control
  - Current Controlled Inverter (CCI) control
- **According to the desired flux operations:**
  - Rotor flux Victor control
  - Stator flux Victor control
  - Air-gap flux (or magnetizing flux) vector control
- **According to the determination of the flux position:**
  - **Direct:** By measuring or observing the flux vector (magnitude, phase)
  - **Indirect:** By controlling the slip frequency

II.4 Flux Orientation Process

There are three types of flux orientation [12]:

- **Rotor flux orientation** with the conditions: $\varphi_{rq} = 0 \Leftrightarrow \varphi_{rd} = \varphi_r$
- **Stator flux orientation** with the conditions: $\varphi_{sq} = 0 \Leftrightarrow \varphi_{sd} = \varphi_s$
- **Air-gap flux orientation** with the conditions: $\varphi_{gq} = 0 \Leftrightarrow \varphi_{gd} = \varphi_g$

In our case, stator flux orientation is the chosen method.

II.5 Types of Vector Control

II.5.1 Direct Control

This type was proposed by Blaschke (1970). In this case, knowledge of the flux magnitude and its phase is required to ensure decoupling between torque and flux, regardless of the transient operating conditions. Indeed, the flux is regulated through feedback control, meaning it must be measured or estimated from the stator voltage and current signals. To obtain information about the flux amplitude and phase, sensors such as Hall Effect probes or measuring coils can be used. These sensors are placed under the stator teeth (in the machine's air gap) [13].

The advantage of this technique is that it is less dependent on parametric variations. However, the drawback of this method is that the sensors are mechanically fragile and cannot operate under harsh conditions such as excessive vibrations and overheating. Additionally, the captured signals are affected by harmonics, and their frequency varies with speed, requiring automatically adjustable filters

II.5.2 Indirect Control

The indirect method was introduced by K. Hasse. The principle of indirect control is based on not measuring (or estimating) the flux amplitude but only its position. It involves estimating the position of the flux vector and regulating its amplitude in an open-loop manner. The voltages or currents responsible for flux orientation and decoupling are determined using a machine model under transient conditions.

This method has been favored by the development of microprocessors, but it is highly sensitive to parametric variations of the machine. It is important to note that the indirect method is simpler to implement and more widely used than the direct method. However, the choice between the two methods depends on the specific application [13.14.15].

II.6 Application of Vector Control to the Doubly-Fed Induction Machine

Unlike the squirrel-cage asynchronous machine, where only stator current measurements are accessible, the doubly-fed slip-ring asynchronous machine offers the advantage of allowing current measurements on both sides. As a result, it provides better control flexibility, leading to improved performance in its control [16].

The expression of the electromagnetic torque of the DFIG allows the asynchronous machine to be considered, from a conversion perspective, as the mechanical association of two DC machines. This facilitates a better interpretation of the coupling problem between the direct and quadrature axis components. Indeed, the expression of the electromagnetic torque for a compensated separately excited DC machine, in the absence of saturation, is given by [17]:

$$T = K\emptyset_{I_f} I_a \quad \text{(II.1)}$$

$\emptyset_{I_f}$: is the flux imposed by the excitation current I_f

I_a: It is the armature current.

According to equation (II.1), the flux depends on the excitation current. Thus, if the flux is constant, torque control is achieved solely through the current. Therefore, torque generation and flux creation are independent.

II.6.1 Choice of Reference Frame

Vector control is based on the choice of a reference frame. In principle, the reference axes can be chosen according to one of the machine's fluxes, namely the stator flux, the rotor flux, or the air-gap flux.

The flux-oriented control consists of regulating the flux using one component of the current and the torque using another component. To orient the stator flux, a (d, q) reference frame must be chosen in such a way that the stator flux is aligned with the axis (od). This allows obtaining an expression for the torque in which the two components of the stator or rotor current are involvedone producing the flux and the other producing the torque. The stator flux orientation leads to:

$\varphi_{sq} = 0 <=> \varphi_{sd} = \varphi_s$

The principle of this type of flux orientation is illustrated in Figure (II.2).

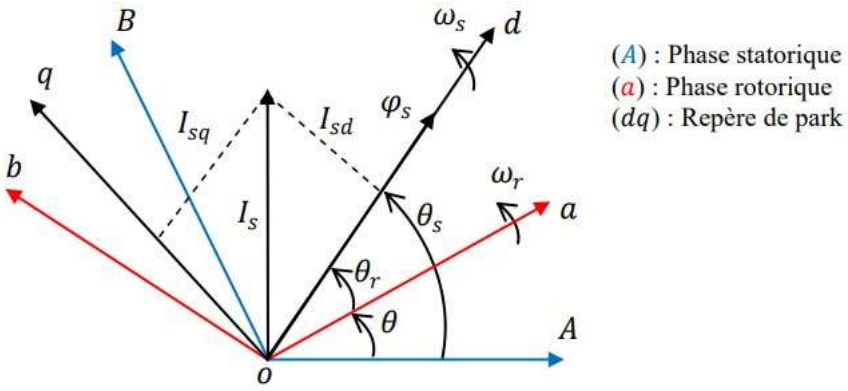

Figure (II.2): Principle of Stator Flux Orientation

Given the adopted working assumptions, this leads us to set the stator current in the d-axis to zero ,$\mathrm{I_{sd}} = 0$. The current and voltage in this axis are then in phase, $V_s = \mathrm{V_{sq}}$ and $I_s = \mathrm{I_{sq}}$ [10].

Modeling our system in steady-state operation as follows:

$$\begin{cases} V_{sd} = R_s I_{sq} \\ V_{sq} = R_s I_{sq} + \omega_s \varphi_{sd} \\ V_{rd} = R_r I_{rd} - \omega_r \varphi_{rq} \\ V_{rq} = R_r I_{rq} + \omega_r \varphi_{rd} \end{cases} \quad \text{(II.3)}$$

The equation of the stator flux is given by substituting equation (II.2) into equation (II.38), we obtain:

$$\begin{cases} \mathrm{I_{sd}} = 0 \\ \varphi_{\mathrm{sq}} = 0 \end{cases} \Longleftrightarrow \begin{cases} \varphi_{sd} = M I_{rd} \\ I_{rd} = \frac{\varphi_{sd}}{M} = \frac{\varphi_s}{M} \\ I_{sd} = -\frac{M}{L_s} I_{rq} \end{cases} \quad \text{(II.4)}$$

The expression of the electromagnetic torque:

$$T_{em} = P \frac{M}{l_s} (\varphi_{sq} I_{rd} - \varphi_{sd} I_{rq}) \quad \text{(II.5)}$$

The stator flux$\varphi_{\mathrm{sq}} = 0$, we obtain:

$$T_{em} = -P \frac{M}{l_s} \varphi_{sd} I_{rq} = -P \frac{M}{l_s} \varphi_s^* I_{rq} \quad \text{(II.6)}$$

$$I_{rq} = -\frac{l_s}{PM} \frac{T_{em}}{\varphi_s^*} \quad \text{(II.7)}$$

From equation (II.3), we have:

$$\omega_s = (\mathrm{V_{sq}} + \frac{R_s M}{L_s} I_{rq}) / \varphi_s^* \quad \text{(II.8)}$$

According to the stator flux equations, we obtain:

$$\mathrm{V_{sd}} = L_s I_{sd} + M I_{rd} \gg I_{sd} = \frac{1}{L_s} (\varphi_{sd} - M I_{rd}) \quad \text{(II.9)}$$

$$\mathrm{V_{sq}} = L_s I_{sq} + M I_{rq} \gg I_{sq} = \frac{1}{L_s} (\varphi_{sq} - M I_{rq}) \quad \text{(II.10)}$$

By substituting equations (II.9) and (II.10) into (I.36), we obtain:

$$\frac{d\varphi_{sd}}{dt} = \mathrm{V_{sd}} + \frac{M}{T_s} I_{rd} - \frac{1}{T_s}\varphi_{sd} \quad \text{(II.11)}$$

$$\frac{d\varphi_{sq}}{dt} = \mathrm{V_{sq}} + \frac{M}{T_s} I_{rq} - \omega_s \varphi_{sd} \quad \text{(II.12)}$$

To express the rotor flux as a function of the stator flux φ_{sd} and the rotor current I_{rd} by substituting equation (II.9) and equation (II.10) into equation (I.38), we obtain the following two equations:

$$\varphi_{rd} = \sigma I_r I_{rd} + \frac{M}{L_s}\varphi_{sd} \quad \text{(II.13)}$$

$$\varphi_{rq} = \sigma I_r I_{rq} + \frac{M}{L_s}\varphi_{sq} \quad \text{(II.14)}$$

By introducing equations (II.13) and (II.14) into equation (I.37), we obtain:

$$\mathrm{V_{rd}} = R_r I_{rd} + \sigma L_r \frac{dI_{rd}}{dt} + \frac{M}{L_s}\mathrm{V_{sd}} - (\omega_s - \omega)\sigma L_r L_{rq} \quad \text{(II.15)}$$

$$\mathrm{V_{rd}} = (R_r + \frac{M^2}{L_s T_S}) I_{rq} + \sigma L_r \frac{dI_{rq}}{dt} + \frac{M}{L_s}\mathrm{V_{sq}} - \frac{M}{L_s}\omega\varphi_{sd} + (\omega_s - \omega)\sigma L_r L_{rd} \quad \text{(II.16)}$$

III.6.2 Direct Vector Control Structure of the DFIM

The block diagram of the direct vector control by stator flux orientation of the doubly-fed induction machine is illustrated in Figure (II.3). This diagram includes four PI-type regulators: one for the flux, one for the speed, and the other two for the current.

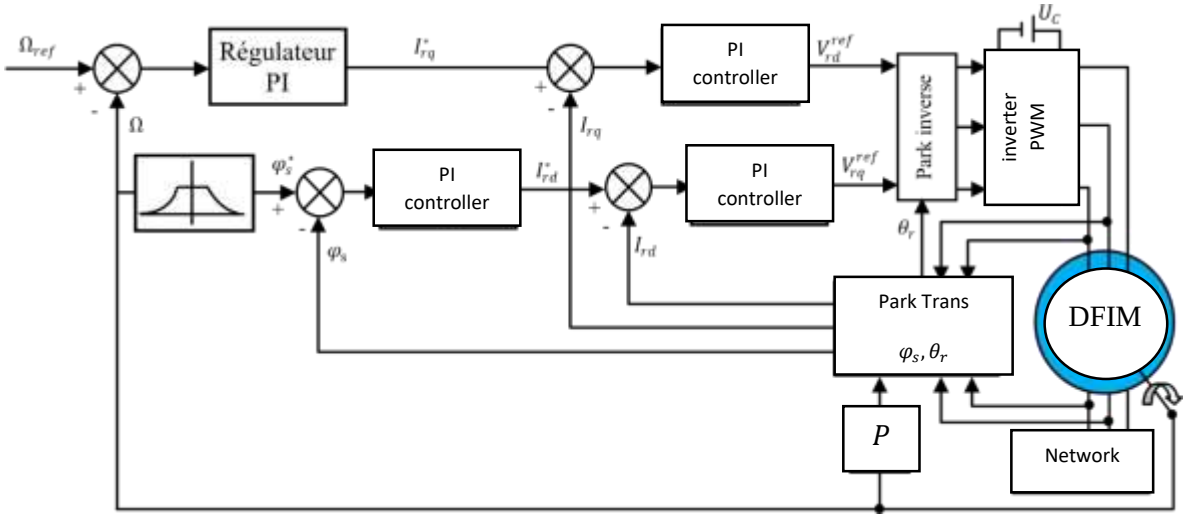

Figure (II.3): Vector Control Structure of the DFIM

III.6.3 Defluxing Block

The operation of the machine is normal up to its nominal values (speed, power, torque). If we want to run the machine at speeds higher than the nominal speed, it becomes overloaded by exceeding its rated power. This is why the magnetic flux of the machine must be reduced as the speed increases beyond its nominal value in order to ensure operation at constant (nominal) power. This operation is called defluxing.

Under these conditions, the machine can be operated at speeds higher than its nominal speed while maintaining constant mechanical power equal to its rated value. In this way, overload and overheating of the machine can be avoided. To achieve this, a reference flux is imposed as defined in [35, 34]:

$$\varphi_s^* = \begin{cases} \varphi_{sn} & si \quad |\omega| \le \omega_n \\ \varphi_{sn}\frac{\omega_n}{|\omega|} & si \quad |\omega| > \omega_n \end{cases}$$

With:

ω_n: $P * \Omega_{sn}$ Is the nominal angular speed of the machine

φ_{sn}:Is the nominal stator flux

Ω_{sn}:Is the nominal mechanical rotational speed of the machine

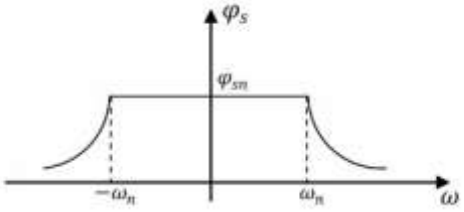

Figure (II.4): Reference stator flux profile (defluxing)

II.6.4 Principle of Decoupling by Compensation

The objective of decoupling is to limit the effect of one input to a single output. We can then model the process as a set of single-input single-output (SISO) systems operating in parallel, where the control actions are non-interacting.

According to equations (II.15) and (II.16), it can be observed that the voltage equations include two coupling terms between the d-axis and the q-axis [10, 18]. Decoupling by compensation requires the introduction of two new control variables, V_{rd} andV_{rq}, such as

$$V_d = V_{rd1} - e_{rd} \tag{II.18}$$

$$V_q = c - e_{rq} \tag{II.19}$$

With:

$$e_{rd} = \delta L_r(\omega_s - \omega)I_{rq} - \frac{M}{L_s}V_{sd} \tag{II.20}$$

$$e_{rd} = \frac{M}{L_s}\omega\varphi_{sd} - \delta L_r(\omega_s - \omega)I_{rd} - \frac{M}{L_s}V_{sq} \tag{II.21}$$

Figure (II.5) shows the reconstruction of voltages V_{rd} and V_{rq} based on e_{rd} and e_{rq}

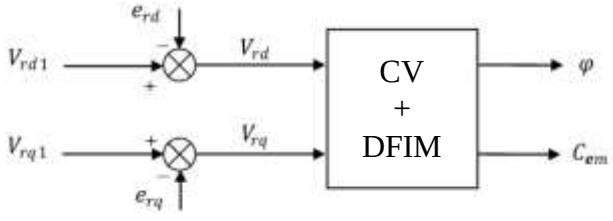

Figure (II.5): Reconstruction of voltages V_{rq} and V_{rd}

His decoupling is based on the introduction of compensatory terms e_{rd} and e_{rq}. An estimate of the actual flux φ_s can be used to calculate e_{rd} and e_{rq}. The controller design is based on linear systems, but an error or drift in the system parameters

Variations in machine parameters lead to the reappearance of coupling and the non-stationarity of the system, and may even cause its destabilization. Therefore, robust controllers are required

II.7 Sizing of the Controllers

For the rotor current, stator flux, and speed control system, we choose to use Proportional-Integral (PI) controllers, as they are simple to implement. This type of controller ensures zero steady-state error through the integration action, while the response speed is determined by the proportional action. The design of the controllers is carried out using the pole placement method [20, 35]

II.7.1 Controller for the Current I_{rd}

The reference is set and measured. It acts on the voltage of V_{rd1}, which is the input current. Regulating this current to a constant value ensures a constant stator flux. The transfer function of the direct rotor current is obtained from equation (II.18) by canceling the compensation termee_{rd}.

$$V_{rd1} = V_{rd} + e_{rd} = R_r I_{rd} + \sigma I_r \frac{dI_{rd}}{dt} = R_r(1 + \sigma T_r.S) I_{rd} \quad \text{(II.22)}$$

$$\frac{I_{rd}}{V_{rd1}} = \frac{\frac{1}{R_r}}{1 + \sigma T_r.S} \quad \text{(II.23)}$$

The block diagram of the I_{rd}^* current control is shown in Figure (II.6*)*

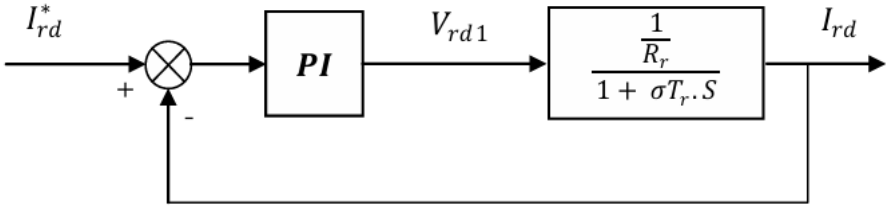

Figure (II.6): Current control diagram of I_{rd}

The transfer function of the PI controller is given by the following equation.

$$PI(s) = K_p + \frac{k_i}{s} \quad \text{(II.24)}$$

The open-loop transfer function (OLTF) of Figure (II.6)

$$FTBO(s)_{I_{rd}} = \frac{K_{id}}{R_r.s}\left(\frac{K_{pd}}{K_{id}}s + 1\right)\frac{1}{1 + \sigma T_r.S} \quad \text{(II.25)}$$

By pole compensation, which is expressed by the condition

$$\frac{K_{pd}}{K_{id}} = \sigma T_r \quad \text{(II.26)}$$

Then the open-loop transfer function is written as follows:

$$FTBO(s)_{I_{rd}} = \frac{K_{id}}{R_r.s} \quad \text{(II.27)}$$

In order to have the behavior of a first-order system whose transfer function is of the form

$$G(s) = \frac{1}{1+\tau s} \tag{II.28}$$

The closed-loop transfer function (CLTF) is given by

$$FTBO(s)_{I_{rd}} = \frac{1}{1+\frac{R_r}{K_{id}}} = \frac{1}{1+\tau s} \tag{II.29}$$

Thus:

$$\tau = \frac{R_r}{K_{id}.} \tag{II.30}$$

From expressions (II.25) and (II.30), we have:

$$\begin{cases} K_{id} = \frac{R_r}{\tau} \\ K_{pd} = K_{id}\sigma T_r = \frac{\sigma T_r}{\tau} \end{cases} \tag{II.31}$$

II.7.2 Controller for the Current I_{rq}

The transfer function of the quadrature rotor current is obtained from equation (II.16) by cancelinge_{rq}.

$$V_{rq1} = V_{rq} + e_{rq} - \frac{M}{L_s}V_{sq} = \left(R_r + \frac{M^2}{L_s T_s}\right) I_{rq} + \sigma L_s \frac{dI_{rq}}{dt} = K_p(1 + \frac{\sigma T_r}{K_p}.s) I_{rq} \tag{II.32}$$

Where

$$K_p = R_r + \frac{M^2}{L_s T_s}$$

Thus

$$\frac{I_{rq}}{V_{rq1}} = \frac{\frac{1}{K_p}}{1+\frac{\sigma L_r}{K_p}.S} \tag{II.33}$$

The current control loop of $Irq*$ can be represented by the block diagram in Figure (II.7).

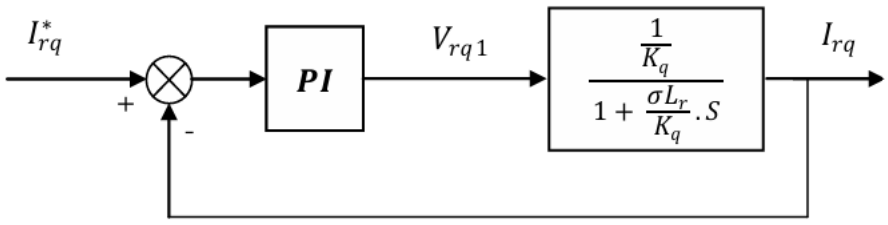

Figure (II.7): Current control diagram of I_{rq}

To determine the two coefficients K_{pd} and K_{iq}, the same procedure used for the I_{rd} current is applied

Thus, we obtain:

$$\begin{aligned} K_{iq} &= \frac{K_p}{\tau} = \frac{R_r + \frac{M^2}{L_s T_s}}{\tau} \\ K_{pq} &= K_{iq}\frac{\sigma L_r}{K_q} = \frac{\sigma L_r}{\tau} \end{aligned} \tag{II.34}$$

II.7.3 Stator Flux Controller

The stator flux orientation allows us to write, based on equation (II.11), we have $V_{sd} = 0$

$$\frac{\varphi_{sd}}{I_{rd}} = \frac{M}{1+T_s s} \tag{II.35}$$

We aim to obtain a first-order response in closed-loop operation. The closed-loop system can be represented by the block diagram in Figure (II.8).

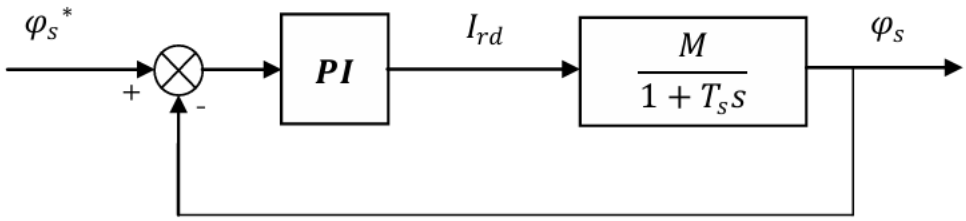

Figure (II.8): Closed-loop stator flux control

Pole compensation allows us to obtain the following condition:

$$T_s = \frac{k_{p\varphi}}{k_{i\varphi}} \tag{II.36}$$

The closed-loop transfer function is now expressed as follows:

$$FTBF(s) = \frac{1}{1+\tau_\varphi s} \tag{II.37}$$

With:

$$\tau_\varphi = \frac{1}{M k_{i\varphi}} \tag{II.38}$$

Based on conditions (II.36) and (II.38), the parameters of the flux controller are:

$$\begin{cases} k_{i\emptyset} = \frac{1}{M\tau_\varphi} \\ k_{p\emptyset} = \frac{T_s}{M\tau_\emptyset} \end{cases} \tag{II.39}$$

II.7.4 Speed Controller

The speed control loop using a PI controller can be represented by the functional diagram in Figure (II.9). The speed controller determines the reference torque in order to maintain the corresponding speed.

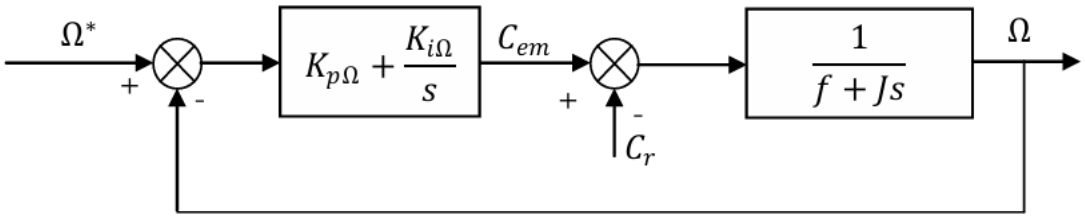

Figure (II.9): Functional diagram of speed control

The mechanical equation gives:

$$\omega = \frac{C_{em} - C_r}{f+Js} \tag{II.40}$$

White

$$\Omega = P\omega \tag{II.41}$$

The closed-loop transfer function, calculated from the previous diagram, is given by:

$$\frac{\Omega}{\Omega^*} = \frac{(k_{p\Omega}s+k_{i\Omega})}{Js^2+(k_{p\Omega}+f)s+k_{i\Omega}} \tag{II.41}$$

This transfer function has a second-order dynamic. By matching the denominator to the canonical form:

$$F(s) = \frac{1}{\frac{1}{\omega_n^2}s^2+\frac{2\xi}{\omega_n}s+1} \tag{II.42}$$

We will have:

$$\begin{cases} k_{i\Omega} = J\omega_n^2 \\ k_{p\Omega} = 2J\xi\omega_n - f \end{cases} \tag{II.43}$$

II.8 Simulation Results

The objective of this step is to control the Doubly-Fed Induction Machine (DFIM) using direct vector control with stator flux orientation. We simulated the system under different conditions to demonstrate the performance of this control method, including variations in speed, load, rotor and stator resistance. In this setup, the stator is directly connected to the grid, while the rotor is supplied through a voltage converter.

II.8.1 Machine Operation During Load Variation

To verify the effectiveness of the vector control, a load of Cr=15 N\m, \ is applied in this test between the instants t=1.5 s and t=2.5 s. The corresponding simulation results are shown in Figure (II.10). The results indicate that with the load variation, all quantities such as speed, torque, fluxes, and currents are affected, demonstrating that the system is perfectly controlled.

We observe the benefits of vector control combined with a PI-type regulation structure, as the rotational speed closely follows its reference. Regarding the torque variation, it can be seen that after a transient phase, it reaches a value that compensates for the applied resistant torque.

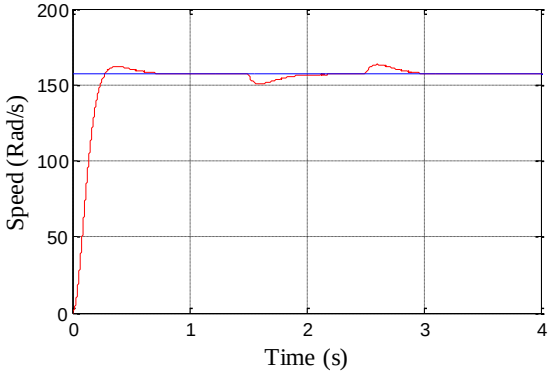

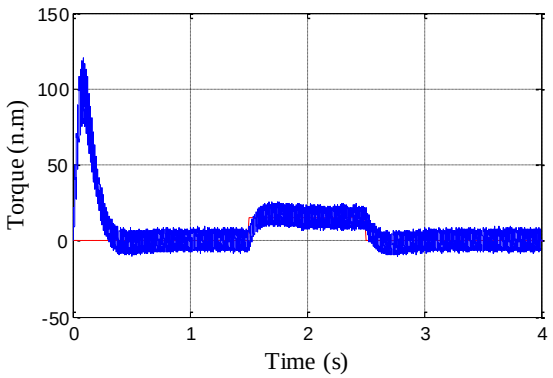

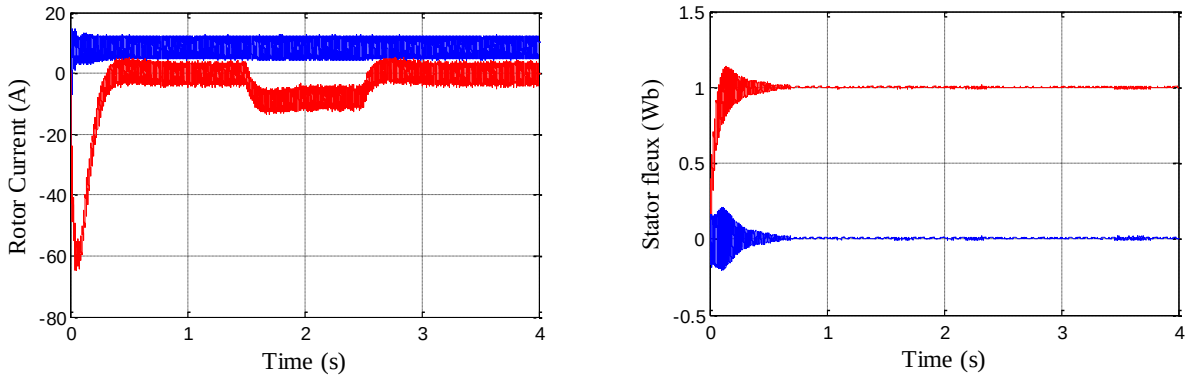

Figure (II.10): Simulation Results During Load Variation

II.8.2 Machine Operation during Speed Variation

The machine is initially loaded with its nominal value C_r=0 N·m and operates at the nominal speed of 157 rad/s. At time t=1.5 s, the direction of rotation is reversed to -157 rad/s, and at t=3 s, the machine operates at a low speed of 50 rad/s. Another load of C_r=15 N.m is applied between t=1.5 s and t=2.5 s. The corresponding simulation results are shown in Figure (II.11), which presents the speed, torque, flux, and direct and in-phase currents generated by the principle of stator flux orientation control.

The speed closely follows its new reference with a slight peak during the transition. The torque tracks its reference accurately, indicating effective decoupling. The flux shows only a minor variation during the speed change.

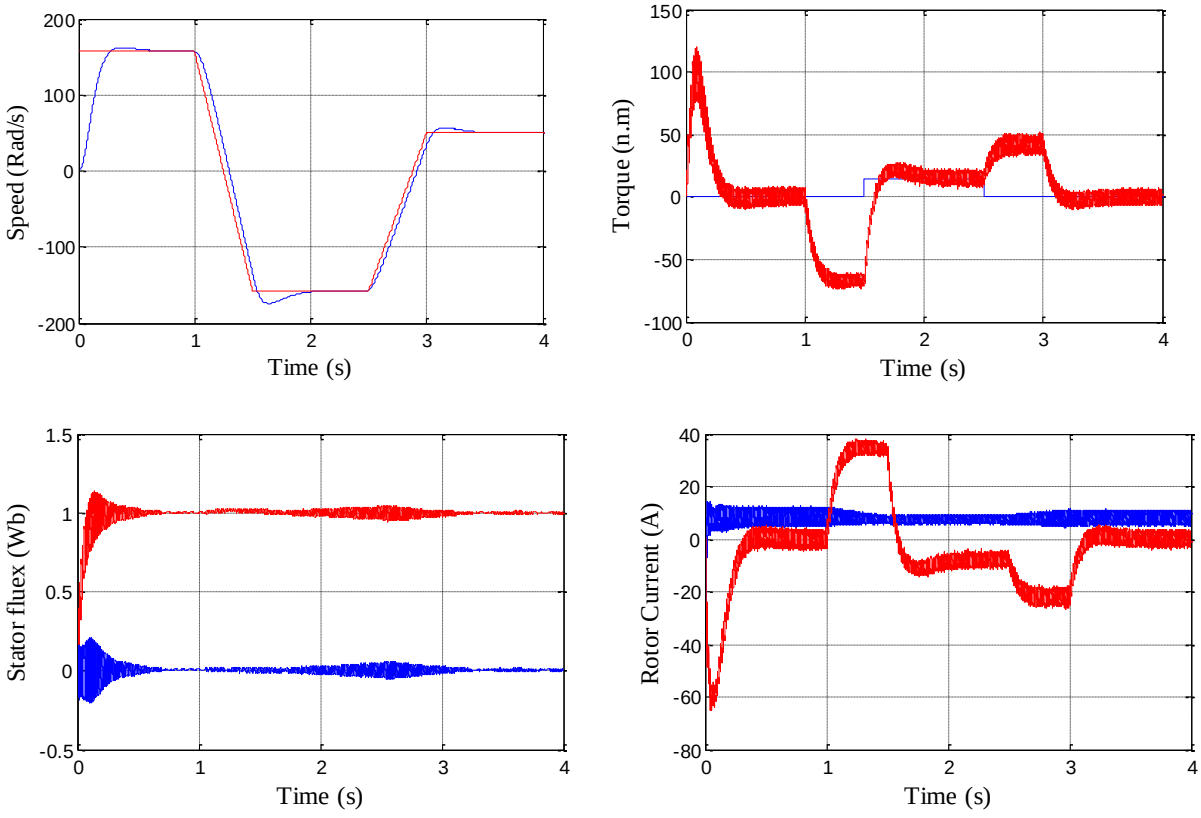

Figure (II.11): Simulation results during speed variation

II.8.3 Operation of the machine during rotor resistance variation

Figure (II.12) presents the simulation results during a +100% variation of the rotor resistance from its nominal value due to machine heating. The variation of R_r is applied between t = 1.5 s and t = 2.5 s. A load torque of C_r=15N.m is also applied during the same time interval, i.e., between t = 1.5 s and t = 2.5 s.

The results show that the variation of the rotor resistance $R_r$does not affect the machine speed, which maintains zero speed error. The noticeable variation is due to the change in the load torque Cr. The torque follows its reference value. The flux exhibits a slight variation in its magnitude, while decoupling is still maintained. The phase currents have a sinusoidal shape, which increases in amplitude with the increase in resistance.

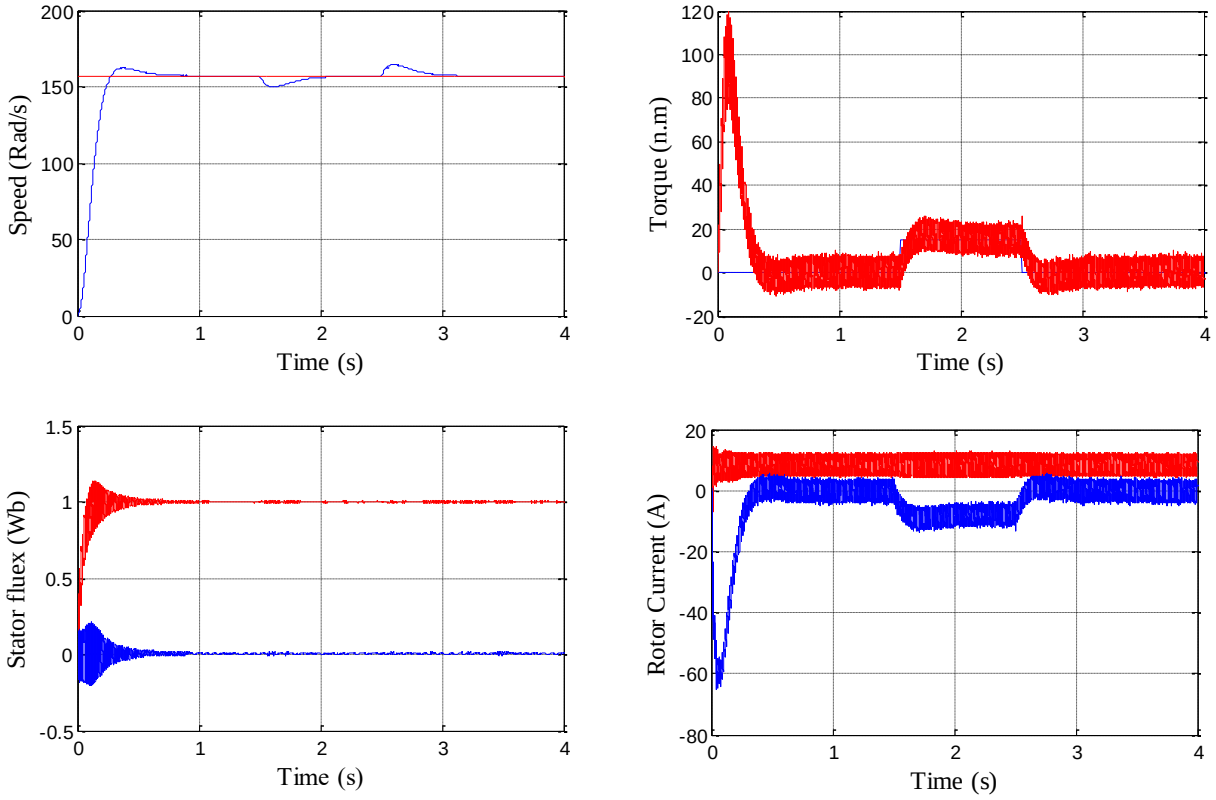

Figure (II.12): Simulation results during the variation of the Rotor resistance

II.8.4 Operation of the machine during stator resistance variation

In this case, we applied a +100% variation of R_s from its nominal value between t = 1.5 s and t = 2.5 s. The results show no change in the speed and flux curves. This proves that the control is robust with respect to the variation of R_s.

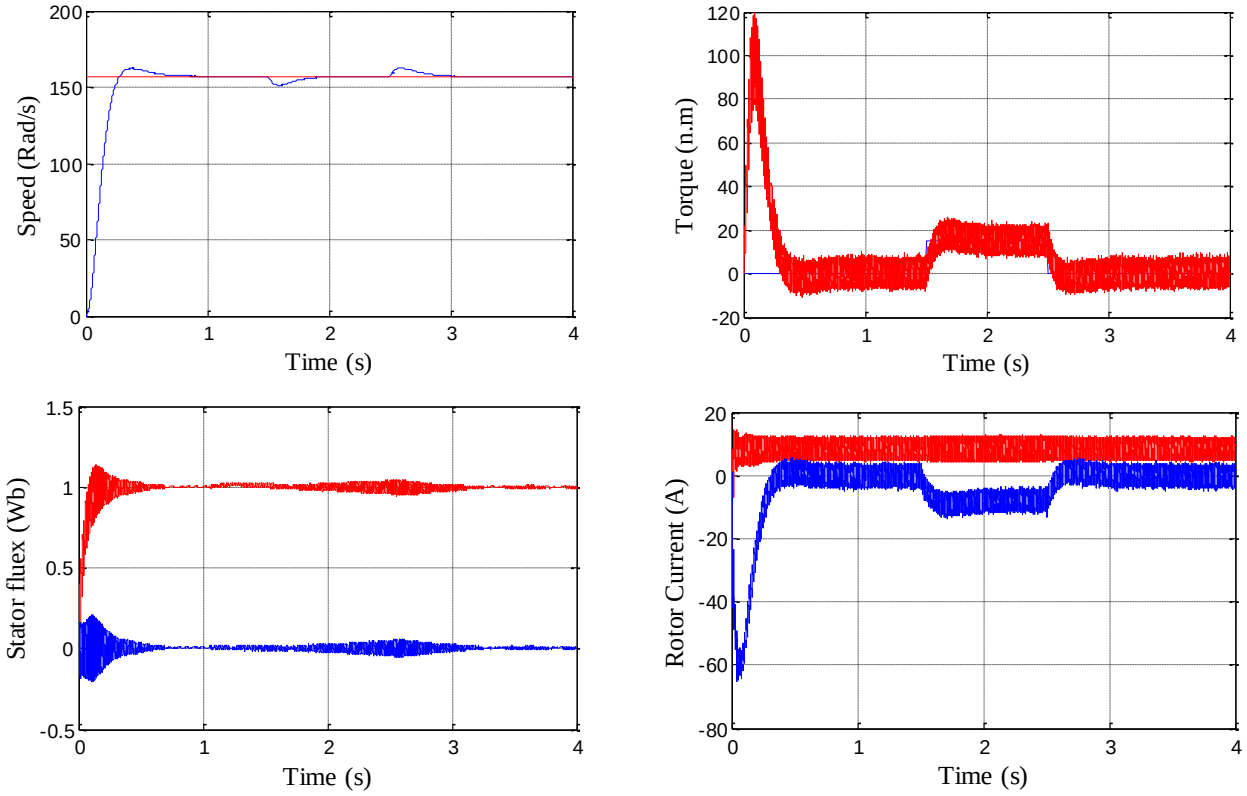

Figure (II.13): Simulation results during the variation of the stator resistance.

II.8.5 Interpretation of the results

Based on the simulation results of the doubly-fed induction machine (DFIM), the effectiveness of the vector control equipped with a PI speed regulator in managing its performance becomes clear. The rotor speed demonstrates a good response and closely follows the reference under various operating profiles, with a notably low tracking error during transient phases that vanishes at steady-state.

A precise orientation of the stator flux was observed, which enhances operational efficiency and optimal machine performance. The electromagnetic torque perfectly tracks the reference torque, ensuring stable and accurate machine operation under different load conditions.

The system exhibited good sensitivity to load disturbances, with a fast disturbance rejection time. The regulator adapts instantaneously when the load torque is applied or removed by promptly adjusting the reference electromagnetic torque effectively.

Regarding mechanical parameters, variations in the moment of inertia had limited impact on the flux orientation but affected the rotor speed, especially during transient phases and disturbances. In contrast, changes in rotor inductance significantly influenced the rotor speed, while having little effect on flux orientation, which showed some variation mainly during transient periods.

For other parameters such as rotor resistance R_r, stator resistance R_s, their variation effects were not accounted for within the current control system.

To further enhance control performance and stability, an advanced technique based on fuzzy logic—a prominent artificial intelligence method will be introduced. The next section aims to present the fundamentals of type-1 fuzzy logic and its application in speed regulation of the doubly-fed induction machine, improving control precision and robustness against uncertainties and disturbances.

II.9 Conclusion

In this chapter, the principle of direct vector control with stator flux orientation for the doubly-fed induction machine (DFIM) was presented and explained. This approach is based on transforming the machine currents into a rotating reference frame (d,q), which allows decoupling the current components and thus enables independent and precise control of each component. Vector control employs state feedback to decouple inputs and outputs, leading to optimal control through transfer functions that directly link currents to their references.

This vector control strategy was implemented alongside a classical PI speed regulator, where the PI controller minimizes the speed error between the reference and the actual machine speed, while the vector control maintains optimal stator flux orientation to ensure stability and efficiency during machine operation. Simulation results demonstrated the system's ability to accurately track the speed reference with stable flux regulation, as well as good disturbance rejection under varying load conditions, highlighting the robustness of vector control in ensuring reliable and steady performance.

However, the classical PI regulator shows limitations when dealing with variations in machine parameters such as resistances or unexpected load torques, which can degrade control quality and reduce system responsiveness to sudden disturbances.

Based on these observations, it becomes essential to explore more flexible and adaptive control solutions capable of handling such parameter variations and disturbances. This need motivates the development of hybrid controllers that integrate artificial intelligence techniques such as fuzzy logic and sliding mode control, which will be discussed in the subsequent chapters.

Chapter III

Fuzzy – SMC – PI Control

III.1 Introduction

The control of electrical machines, particularly the Doubly-Fed Induction Machine (DFIM), represents a major challenge in the field of modern electromechanical systems. Thanks to its ability to operate in both motor and generator modes with independent control of active and reactive power, the DFIM is widely used in applications such as wind energy.

However, the complexity of the DFIM's dynamic behavior, especially in the presence of disturbances, parameter variations, or inherent nonlinearities, makes it necessary to develop advanced control strategies that can ensure robustness, performance, and adaptability.

In this context, classical control techniques, such as the Proportional-Integral (PI) controller, show their limitations, particularly in terms of dynamic performance and robustness against uncertainties. To overcome these shortcomings, modern approaches such as Sliding Mode Control (SMC) and Fuzzy Logic have been introduced. SMC offers remarkable robustness against uncertainties and disturbances, but it often suffers from the "chattering" phenomenon—an undesirable oscillation that can damage actuators. On the other hand, Fuzzy Logic allows for modeling uncertainty and imprecision in the system without requiring an accurate mathematical model.

The integration of these three approaches into a hybrid Fuzzy-PI-SMC controller aims to combine the advantages of each the simplicity and efficiency of the PI controller, the robustness of Sliding Mode Control, and the adaptability of Fuzzy Logic.

This chapter is dedicated to the development, modeling, and analysis of a hybrid control strategy applied to the DFIM. We present the fundamental principles of each technique, their combined implementation, as well as the benefits offered by this hybridization in the context of DFIM speed control.

III.2 Fuzzy Logic

Fuzzy Logic is a branch of artificial intelligence developed to handle uncertain and imprecise information, and to represent vagueness and approximation in dynamic and nonlinear systems. It extends classical Boolean logic, which relies only on binary values (0 and 1), by allowing degrees of truth ranging between 0 and 1. Professor Lotfi A. Zadeh is considered the pioneer of this concept, having introduced it in his seminal 1965 paper titled *"Fuzzy Sets,"* which laid the foundation for numerous applications in intelligent control and complex systems [5].

The core idea of fuzzy logic is to enable systems to deal with vague and imprecise values using concepts similar to human reasoning, such as *"warm," "fast,"* or *"strong,"* rather than relying solely on strict definitions. In traditional systems, decisions are based on exact thresholds, while in fuzzy logic, elements can partially belong to multiple fuzzy sets simultaneously.

A fuzzy logic system typically comprises four main stages [20]:

1. **Fuzzification**, where crisp input values are converted into fuzzy values using membership functions;
2. **Rule Base**, which contains a set of rules based on human knowledge or empirical data;
3. **Inference Engine**, which deduces results from these rules;
4. **Defuzzification**, which transforms the fuzzy output into a precise action or control signal.

Fuzzy logic is widely applied in various domains, especially in industrial control systems such as temperature regulation, motor speed control, and electrical systems like the Doubly-Fed Induction Machine (DFIM). It is also used in fields like medicine, robotics, smart home appliances, image processing, and natural language processing [19][21][22].

The advantages of fuzzy logic include the simplification of control system design, particularly when building an exact mathematical model is difficult. It also offers smooth and flexible responses under varying conditions. However, one of its main drawbacks is the heavy reliance on human expertise to define the rule base and membership functions, which may impact system precision and performance [19][20].

III.2.1 Fuzzification in Fuzzy Logic

Fuzzification is the first stage in a fuzzy logic system, where precise numerical inputs (crisp inputs) are transformed into fuzzy values. The goal of this process is to represent quantitative values with imprecise linguistic terms that the system can interpret, enabling it to handle uncertainty and ambiguity often present in real-world applications.

This process relies on the use of membership functions, which are mathematical functions that define the degree to which a numerical input belongs to a particular fuzzy set. The membership degree ranges between 0 and 1. In this way, a single numerical value can be represented by multiple degrees of belonging to different linguistic sets, allowing for a more flexible and gradual interpretation of inputs [23].

Various types of membership functions are used in fuzzification, the most common being: triangular, trapezoidal, and Gaussian. The choice of function depends on the system's nature, the type of data, and the level of modeling precision required [24].

This stage is crucial as it prepares the input data to be processed in the fuzzy inference system, where decisions and control actions are based on linguistic rules rather than exact equations. The ability to represent an input value with multiple degrees of membership to different sets is what gives fuzzy logic systems their flexibility and effectiveness in handling complex and nonlinear problems [5].

III.2.2. Rule Base in Fuzzy Logic

The Rule Base is one of the core components of a fuzzy inference system. It stores a set of fuzzy IF-THEN rules used to make decisions or perform control actions based on fuzzified inputs. These rules are typically derived from human expertise or empirical knowledge and are expressed in linguistic form, suchas: "IF the speed is high AND the torque is low, THEN the voltage should be medium" [23].

Each rule connects a set of input conditions to a specific output action using linguistic variables rather than numerical values. These conditions are evaluated based on the fuzzy input values produced by the fuzzification process. The Rule Base is the foundation of rule-based inference, allowing the system to operate in a way that resembles human reasoning [24].

A typical Rule Base includes:

- A collection of fuzzy IF-THEN rules.
- Linguistic variables for inputs and outputs.
- Logical connectors like AND and OR to combine multiple conditions within a rule.

The rules are usually constructed manually by experts who understand the behavior of the system. Alternatively, they can be generated or refined using experimental data. The more comprehensive the Rule Base is in covering various system scenarios, the more accurate and effective the fuzzy system becomes in its decision-making [24].

The Rule Base essentially serves as the knowledge base of the fuzzy system. It translates human understanding or observations into structured logic that can be processed by the fuzzy inference engine. This capability allows fuzzy systems to handle complex or uncertain environments in a manner similar to human problem-solving [23].

III.2.3 Inference Engine in Fuzzy Logic

The Inference Engine is the core component responsible for executing the reasoning process in a fuzzy logic system. It operates by applying the Rule Base to the fuzzified input values, in order to derive conclusions or decisions [23].

This engine identifies which rules are applicable to the current fuzzy inputs and evaluates the degree to which each rule is satisfied by computing the membership values that fulfill the rule's conditions. Then, it determines the fuzzy output of each rule and aggregates all valid rule outputs to produce a combined fuzzy result [25].

The inference process typically uses one of two common fuzzy reasoning models:

- **Mamdani Inference:** This is the most widely used approach in practical applications. It employs fuzzy membership functions for both inputs and outputs, and uses operations like "minimum" (min) and "maximum" (max) for rule evaluation and aggregation [24].
- **Sugeno (Takagi-Sugeno) Inference:** This method is favored when higher numerical precision is needed. The outputs of the rules are not fuzzy sets but instead mathematical functions (often linear or polynomial) [25].

The Inference Engine performs logical operations such as AND, OR, and NOT using mathematical equivalents (e.g., min, max, product) to process relationships between rule conditions. Then, the results of the fired rules are aggregated to produce a single fuzzy output, which is passed on to the Defuzzification stage [23].

In summary, the Inference Engine is the reasoning core of the system, responsible for decision-making based on the rule-based knowledge and for managing multi-condition scenarios in a flexible, human-like manner [25].

III.2.4 Defuzzification in Fuzzy Logic

Defuzzification is the final stage in a fuzzy logic system. In this phase, the fuzzy output obtained from the inference process is converted into a precise numerical value (crisp output) that can be used by the physical system, such as a control signal sent to a motor or actuator [23].

Since the results of the inference engine are typically fuzzy sets—formed by aggregating the outcomes of multiple rules—they cannot be directly applied in physical or digital systems. This makes defuzzification an essential step to transform those fuzzy results into meaningful numerical values [24].

Several defuzzification methods exist, with the most common being:

- **Centroid Method (Center of Gravity):** This is the most widely used method. It calculates the center of the area under the output membership function curve as the final crisp value. While accurate, it often involves complex integration [24].
- **Center of Area (COA):** Similar to the centroid method, but it simplifies the fuzzy shape into basic regions for balancing.
- **Mean of Maximum (MOM) or First of Maximum (FOM):** These methods consider only the output values with the highest membership degree. They are computationally less intensive but generally less accurate [25].

The precision of a fuzzy control system heavily depends on the appropriate choice of defuzzification method. This choice is influenced by the application's requirements—whether higher accuracy or faster computation is needed—and by the complexity of the membership functions involved [23].

Ultimately, defuzzification serves as the bridge between fuzzy linguistic reasoning and the real physical system. It transforms fuzzy outputs into crisp signals that can be used in practical implementation [24].

III.3 Sliding Mode Control (SMC)

Classical control techniques (such as PI or PID controllers) require a perfect knowledge of the system model to be regulated. These approaches lead to control laws whose performance is highly dependent on the accuracy of the dynamic model used to describe the system's behavior. Modeling errors or parameter uncertainties can degrade the performance of the control system since they directly affect the computation of the control law.

Sliding Mode Control (SMC) is a particular operating mode of variable structure systems. SMC remains one of the most extensively studied control techniques in research due to its robustness and simplicity [26, 27–28]. These key features are the main reasons why this method continues to attract significant interest.

In this section, we present the fundamental elements of the variable structure control framework. First, we briefly explain the principle of this control method and the selection of the sliding surface. Then, we present the different structures of sliding mode control.

III.4. Theory of Sliding Mode Control

Variable structure control is a nonlinear and discontinuous type of control. It involves an intentional modification of the system's topology, forcing the system's state trajectory (the system dynamics) to switch around a predefined (or desired) hyper surface, called the sliding surface, and to slide along it until reaching the equilibrium point, thanks to a switching device and logic [26, 29].

When the representative point of the system's motion is maintained on the sliding surface (Figure (III.3)), the system is said to be in sliding mode and is then governed by the dynamics of a reduced and free system. Thus, as long as the sliding conditions are satisfied, the system's dynamics

remain insensitive to modeling uncertainties, parameter variations, and certain external disturbances.

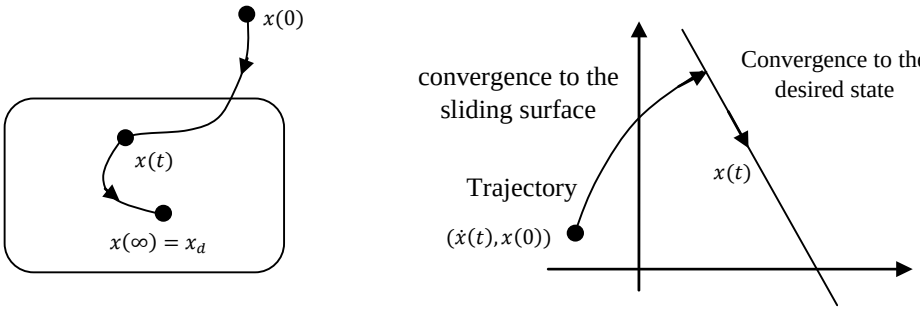

Figure (III.1): Convergence of the Sliding System

III.4.1 Objective of Sliding Mode Control

The objective of sliding mode control can be summarized in two key points:

- To synthesize a sliding surface S(x ,t) such that all system trajectories follow a desired behavior of tracking, regulation, and stability.
- To determine a control law (switching law) U(x ,t) that is capable of driving all state trajectories toward the sliding surface and maintaining them on this surface.

III.4.2 Existence Condition of the Sliding Mode

The sliding mode exists when continuous switching occurs between U_{max} and U_{min}. This phenomenon is illustrated in Figure (III.2) for the case of a second-order control system with two state variables $x_1$and x_2[30, 31].

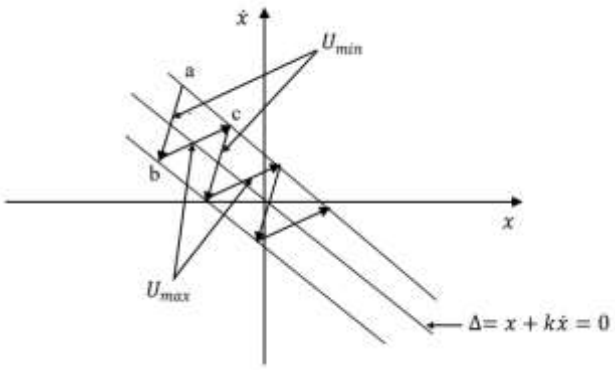

Figure (III.2): Demonstration of the Sliding Mode

First, consider a hysteresis around the switching law S(x) =0 (the dashed line). The switching's occur along two parallel lines offset by ±ΔS.

A trajectory with $U = U_{max}$ touches point "a" which is the lower switching threshold. If, with $U = U_{min}$, the trajectory is directed inward within the hysteresis band, it reaches point "b," the upper switching threshold, where the control switches back to $U = U_{min}$. If the trajectory then reverses direction downward, the process repeats.

Thus, there is a continuous movement within the hysteresis zone. Consequently, the switching law performs an infinitely small oscillation around S(x) =0, and the vector x follows a trajectory that respects this condition.

III.5 Design of Sliding Mode Control

The design of sliding mode controllers systematically addresses stability issues and desired performance. Implementing this control method mainly requires three steps: selecting the sliding surface, establishing the conditions for existence and convergence, and determining the control law [32, 33–34]

III.5.1 Choice of Sliding Surfaces

The choice of the sliding surface involves not only determining the necessary number of these surfaces but also their shape, depending on the application and the desired objective.

In general, for a system defined by the following state-space equation:

$$\begin{cases} \dot{x}(t) = f(x,t) + g(x,t)u(t) \\ \quad y = C^t x,\ y \in R^m \end{cases} \tag{III.3}$$

For an output vector **y** of dimension mmm, it is necessary to choose mmm sliding surfaces. Two main approaches exist: phase space and state space.

In the state space approach, the switching law method is based on state feedback, but it typically results in slow transient response and is difficult to design.

In the phase space approach, the switching function S(x) is a scalar function that guides the controlled variable **y** to slide along the surface toward the origin of the phase plane, representing the desired dynamic behavior of the system.

J. J. Slotine proposed a general equation to define the sliding surface that ensures convergence of the variable **y** to its desired value:

$$S(x) = (\frac{\partial}{\partial t} + \lambda_x)^{r-1}.e(x) \tag{III.4}$$

$e(x) = x_{ref} - x$: The deviation of the variable to be controlled.

λ_x: A positive constant that represents the desired control bandwidth.

r : Relative degree: the number of times the output must be differentiated before the control input explicitly appears.

$For\ r: 1, S(x) = e(x)$

$For\ r: 2, S(x) = \lambda_x e(x) + \dot{e}(x)$

$For\ r: 3, S(x) = \lambda_x^2 e(x) + 2\lambda\dot{e}(x) + \ddot{e}(x)$

S(x) is a linear differential equation whose unique solution is $e(x) = 0$.In other words, the challenge is reduced to a trajectory tracking problem, with the objective of maintaining$S(x) = 0$. This is equivalent to an exact linearization of the error while satisfying the convergence condition.

The purpose of the exact linearization of the error is to force the error dynamics (reference – output) to follow the dynamics of an autonomous linear system of order r.

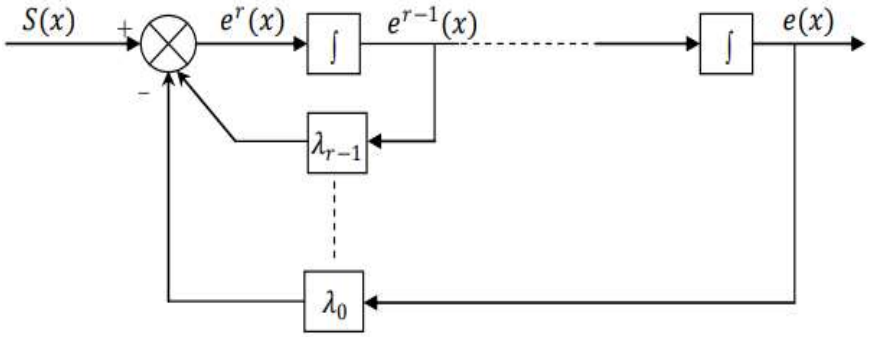

Figure (III.3): Exact Linearization of the Error

III.5.2 Convergence Conditions

The convergence conditions ensure that the system dynamics converge toward the sliding surfaces. Based on the literature, two main conditions are retained; these correspond to the convergence mode of the system's state.

III.5.2.1 Direct Switching Function

This was proposed and studied by Emelyanov and Utkin. The idea is to assign the surface a converging dynamic toward zero. It is

$$\dot{S}(x)S(x) < 0 \qquad \text{(III.5)}$$

III.5.2.2 Lyapunov Function

The Lyapunov function is a positive scalar function $V(x) = 0$ defined for the system's state variables. It is used to evaluate the performance of the control strategy in terms of robustness. It guarantees the stability of the nonlinear system and ensures the convergence of the controlled variable toward its reference value. It takes the following form [36].

By defining the Lyapunov function as:

$$V(x) = \frac{1}{2}s^2(x) \qquad \text{(III.6)}$$

Where S(x) describes the distance of the point $\boldsymbol{x}$ from the sliding surface S(x) =0.

In order for the Lyapunov function to decrease, we must ensure that:

$$\dot{V}(x) = S(x).\dot{S}(x) \qquad \text{(III.7)}$$

The control law must cause this function to decrease, i.e ,$\dot{V}(x) < 0$.

The idea is to choose a scalar function S(x) to ensure the attraction of the variable to be controlled toward its reference value, and to design a control input "u" such that the square of the surface corresponds to a Lyapunov function.

In order for the function V(x) to decrease, it is sufficient to ensure that its derivative is negative.

Hence, the convergence condition is expressed by:

$$S(x).\dot{S}(x) < 0 \qquad \text{(III.8)}$$

This equation shows that the square of the distance to the surface, measured by $S^2(x)$ continuously decreases, forcing the system's trajectory to move toward the surface from both sides (Figure III.6). This condition assumes an ideal sliding mode regime.

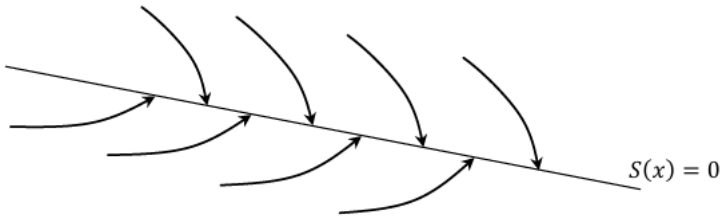

Figure (III.4)*:* State Trajectory with Respect to the Sliding Surface

III.5.3 Determination of the Control Law

Once the sliding surface and the convergence criterion have been defined, the next step is to determine the control law needed to bring the controlled variable back to the sliding surface, and then to its equilibrium point, while maintaining the condition for the existence of sliding modes.

One of the key assumptions in the design of variable structure systems controlled by sliding modes is that the control must switch instantaneously between U_{max} and U_{min}, depending on the sign of the sliding surface (Figure III.5).

In this case, very high-frequency oscillations, known as "chattering", appear during the sliding mode.

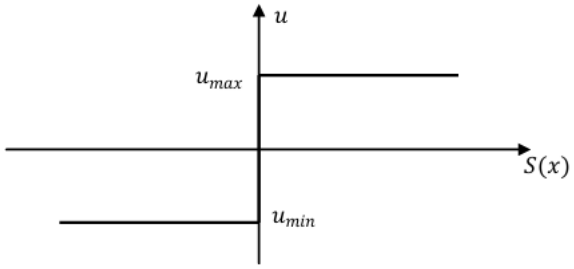

Figure (III.5): Control Applied to Variable Structure Systems

III.6 Application of Sliding Mode Control to the DFIM

This study aims to apply sliding mode control for speed of the doubly-fed induction machine (DFIM), based on a model oriented by the stator flux. The system is decoupled along the d and q axes and controlled using a cascade control structure.

III.6.1 Speed control surface

The speed error is defined by

$$e = \Omega_{ref} - \Omega \tag{III.9}$$

To control the speed, we take the following approach, and the various forms of the speed control equation can be obtained as follows:

$$S(\Omega) = \ e = \Omega_{ref} - \Omega \tag{III.10}$$

The derivative of the surface is

$$\dot{S}(\Omega) = \dot{\Omega}_{ref} - \dot{\Omega} \quad \text{(III.11)}$$

By substituting the expression

$$\dot{S}(\Omega) = \dot{\Omega}_{ref} + \frac{1}{j}\left(\frac{P.M}{L_s}\varphi_{sd} I_{rq} + f\Omega + C_r\right) \quad \text{(III.12)}$$

We take:

$$I_{rq} = I_{rq}^{eq} + I_{rq}^{n} \quad \text{(III.13)}$$

The control clearly appears in the following equation:

$$\dot{S}(\Omega) = \dot{\Omega}_{ref} + \frac{1}{j}\left(\frac{P.M}{L_s}\varphi_{sd}(I_{rq}^{eq} + I_{rq}^{n}) + f\Omega + C_r\right) \quad \text{(III.14)}$$

During the sliding mode and in steady state, we have: $S(\Omega) = 0, \dot{S}(\Omega) = 0 \; and \; I_{rq}^{n} = 0$

The equivalent control equation becomes:

$$I_{rq}^{eq} = \frac{jL_s}{PM\varphi_{sd}}\left(\dot{\Omega}_{ref} + \frac{f}{j}\Omega + \frac{C_r}{j}\right) \quad \text{(III.15)}$$

During the reaching phase, the condition $S(\Omega)\dot{S}(\Omega) < 0$ must be satisfied. By substituting the expression of the equivalent control into the expression of the surface derivative, we obtain:

$$\dot{S}(\Omega) = \frac{PM\varphi_{sd}}{L_s} I_{rq}^{n} \quad \text{(III.16)}$$

We take:

$$I_{rq}^{n} = KI_{rq}.\text{sign}\,(S(\Omega)) \quad \text{(III.17)}$$

To verify the system's stability condition, the constant KI_{rq} must be negative

III.6.2 structure the SMC for speed control

This figure illustrates the structure of the Sliding Mode Controller (SMC) for controlling the currentI_{rq}, where two control components are generated: the equivalent current I_{rq} and the discontinuous current I_{rq}, aiming to accurately track the reference speed Ω_{ref}\while ensuring disturbance rejection.

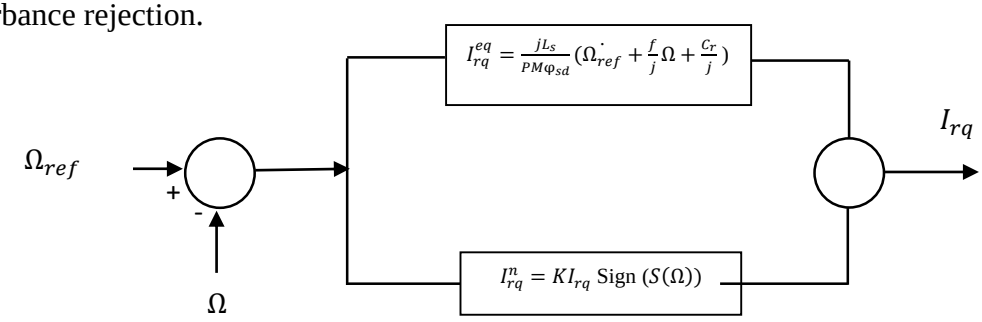

Figure (III.6) :structur the SMC for speed control

III.7 FUZZY-SMC-PI CONTROL

With the advancement of modern electric drive system requirements, there is an increasing need for advanced control strategies characterized by accuracy, speed, and robustness against disturbances. The Doubly-Fed Induction Machine (DFIM), also known in French as Machine Asynchrony à Double Alimentation (MADA), is one of the most prominent machines used in

renewable energy applications, especially in variable-speed wind power systems, due to its broad speed control range and high efficiency.

In this context, a hybrid control structure known as FUZZY-SMC-PI has been proposed, which integrates:

- Sliding Mode Control (SMC) to provide fast response and strong robustness against disturbances.
- Proportional-Integral (PI) Control to ensure complete elimination of steady-state error.
- Fuzzy Logic as an intelligent mechanism to enable smooth switching between SMC and PI depending on system conditions .

This strategy combines the advantages of each technique to overcome their individual limitations. While SMC offers fast response but suffers from chattering that affects stability, PI control achieves steady-state accuracy but with overshoot and longer settling time, fuzzy logic acts as an intelligent coordinator to ensure enhanced overall performance [37].

The objective of this chapter is to implement the FUZZY-SMC-PI structure on the Doubly-Fed Induction Machine, by analyzing the proposed architecture, determining its integration with rotor-side control circuits, and demonstrating the system's dynamic behavior under different operating conditions. Subsequently, the performance of this strategy will be evaluated through numerical simulation and compared with conventional control approaches.

III.7.1 Fuzzy logic control

Fuzzy-SMC-PI strategy is developed by dividing the control region into three different regions as shown in Fig. 1 where *he* is the system's error. The first region involves pure SMC strategy. This region is responsible in bringing the system state to the targeted state as quickly as possible. This is followed by mixed strategy region which consists of SMC and PI strategies working in tandem through fuzzy logic to produce a single controller output. The objective of this region is to subdue any probable over-shoot prior to the steady state. The third and the final region is the pure PI strategy region. The output from this region serves to keep the steady error to a minimum or eliminates it totally.

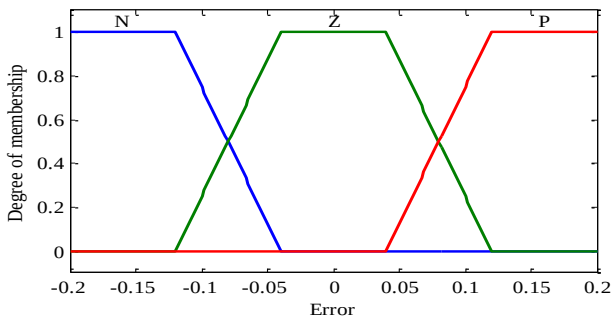

Figure (III.7): Fuzzy logic membership functions

From the previous definition of the controller, it follows that the linguistic rules of the fuzzy logic supervisory controller should be defined as follows:

$$\begin{cases} Rule\ 1 \quad IF\ e\ \ is\ Negativ\ THEN \quad i = I_{SMC} \\ Rule\ 2 \quad IF\ \ e\ \ is \quad Zero\ THEN \quad i = I_{PI} \\ Rule\ 3 \quad IF\ e\ \ is\ positiv \quad THEN \quad i = I_{SMC} \end{cases} \tag{III.18}$$

Where e is the speed error and acts as the input to the fuzzy logic controller. The linguistic terms N (Negative), Z (Zero), and P (Positive) are defined by the membership functions shown in Figure (III.9) the symbol μ represents the degree of membership. The control inputs i_{PI} and i_{SMC} are the outputs of the PI and SMC controllers, respectively, and are calculated as follows:

$$\begin{cases} I_{PI} = k_p.e + k_i.\int edt \\ I_{SMC} = g.sign\ I \end{cases} \tag{III.19}$$

Where g is the SMC constant control gain and *sign* is the signum function. Note that the proposed sliding surface is designed to be the system's error, i.e. $s = e$. Figure (III.10) represents block diagram for implementation.

III.7.2 FUZZY-SMC-PI CONTROL STRUCTURE:

Fuzzy SMC-PI is basically a combination of SMC and PI through fuzzy logic. The advantage of such strategy is as follows. The SMC is responsive during transient state but it has an inherent chattering problem. This chattering phenomenon continuously created noise even under steady state. Thus zero steady state error is not attainable with control strategy using SMC methodology alone. On the other hand, with PI control strategy, zero steady state error is achievable but the PI control strategy is not all that ideal too. It has a significant overshoot problem and has a longer settling time and rise time. Comparatively, it is less responsive to SMC control strategy. The combination of both control strategies through fuzzy logic provides a mean to create a hybrid control strategy that produce minimum overshoot, faster settling time and an almost chatter free system. The resulting hybrid system operates by sliding between SMC and PI mode depending on the condition imposed by external factors such as load.

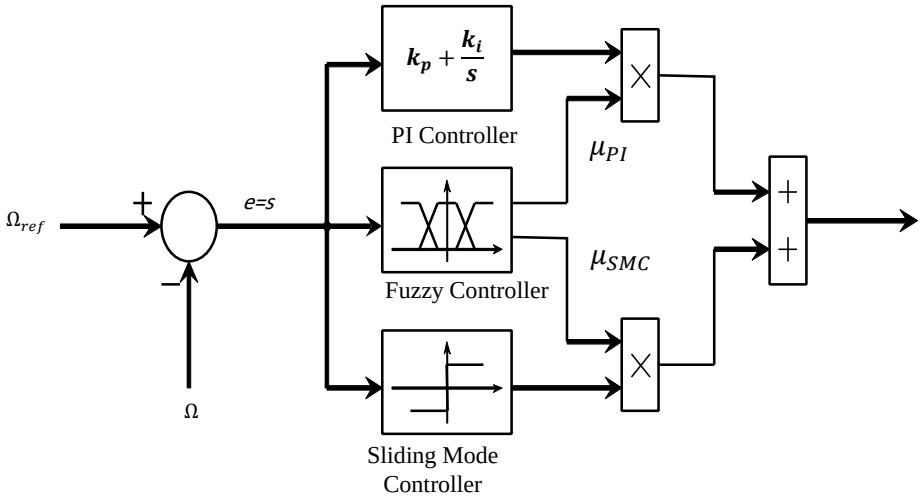

Figure (III.8) Structure of the FUZZY-SMC-PI Control of the DFIM

III.7.3. Structure of FUZZY-SMC-PI Control for DFIM

Figure (III.8) illustrates the block diagram of the direct vector control based on stator flux orientation of the doubly-fed induction machine. This diagram includes four PI controllers: one for flux control, one FUZZY-SMC-PI for speed control, and two for current control

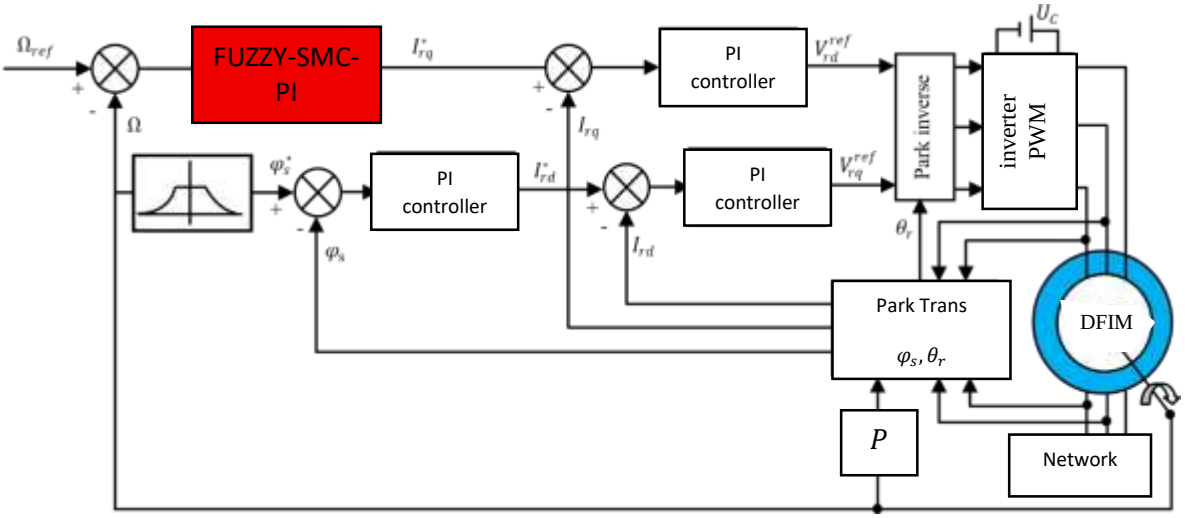

Figure (III.9): Structure of FUZZY-SMC-PI Control for DFIM

III.8 Simulation Results

The objective of this step is to apply a hybrid control strategy combining Sliding Mode Control (SMC), Proportional-Integral (PI) control, and fuzzy logic to enhance the performance of the Doubly-Fed Induction Machine (DFIM). Through simulation, we evaluate the efficiency and robustness of this approach under various operating scenarios, including speed reference changes, load disturbances, and parameter variations. This method aims to improve dynamic response, reduce steady-state error, and increase robustness against uncertainties, offering a more flexible and intelligent control structure compared to conventional techniques

III.8.1 Machine Operation during Load Variation

A load torque of $C_r = 15\, n.m$ is applied between t=1.5s and t=2.5 s. The results show slight changes in speed, torque, and flux during the load variation, but the system remains stable, with the speed accurately tracking the reference thanks to the SMC-PI-Fuzzy control.

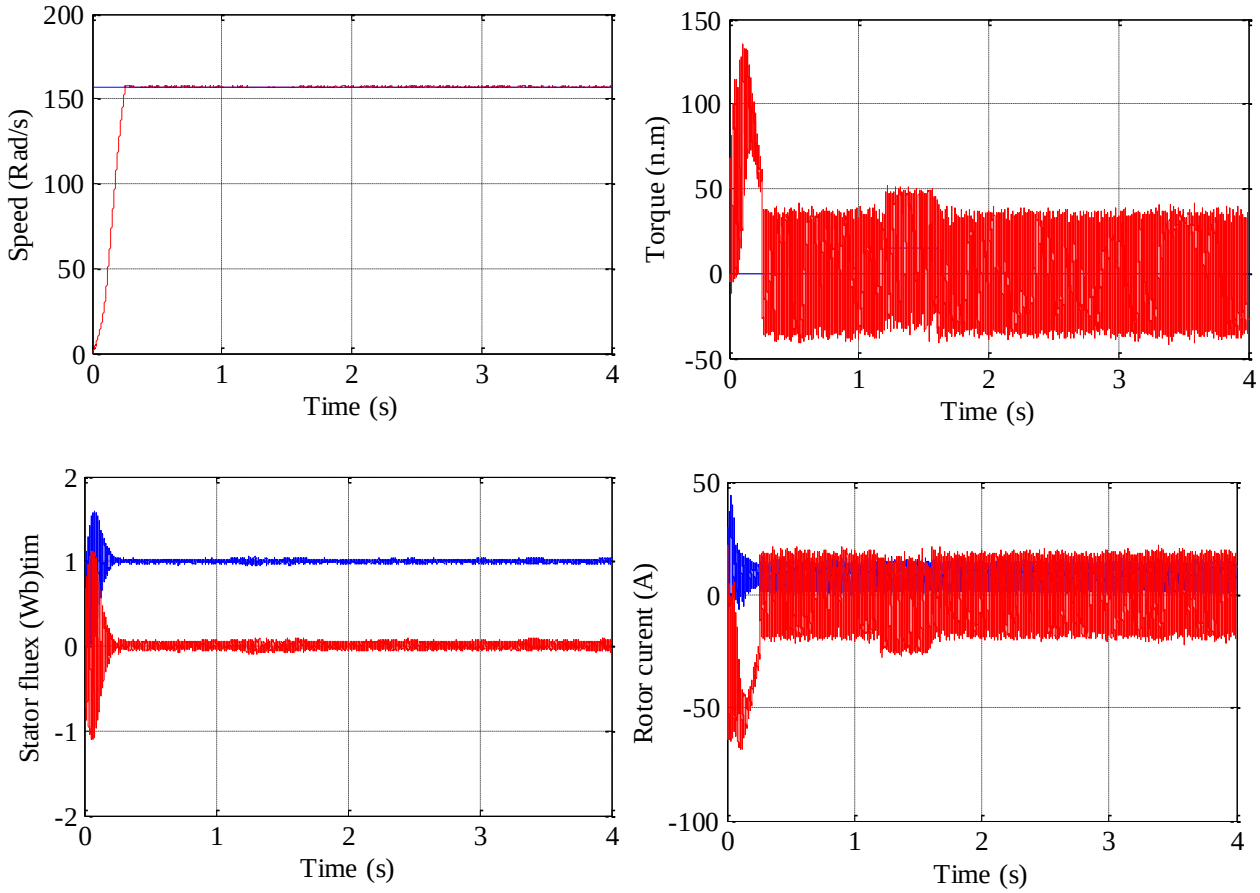

Figure (III.10): Simulation Results During Load Variation

III.8.2 Machine Operation during Speed Variation

The machine speed is changed from 157 to –157 and then to 50 rad/s at different times, with a load of $C_r = 15\,n.m$ between t=1.5s and 2.5s. The speed follows the reference smoothly, and the torque and flux stay stable, reflecting the effectiveness of the SMC-PI-Fuzzy control.

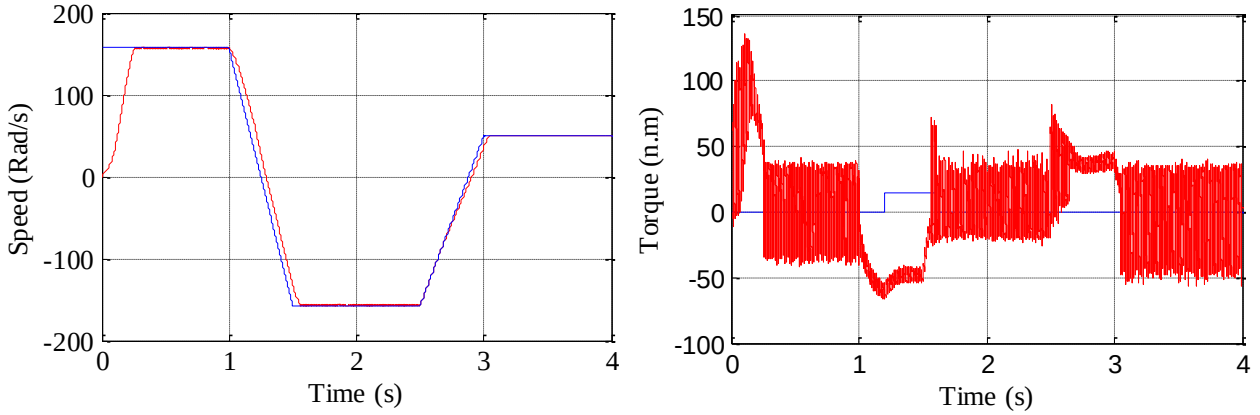

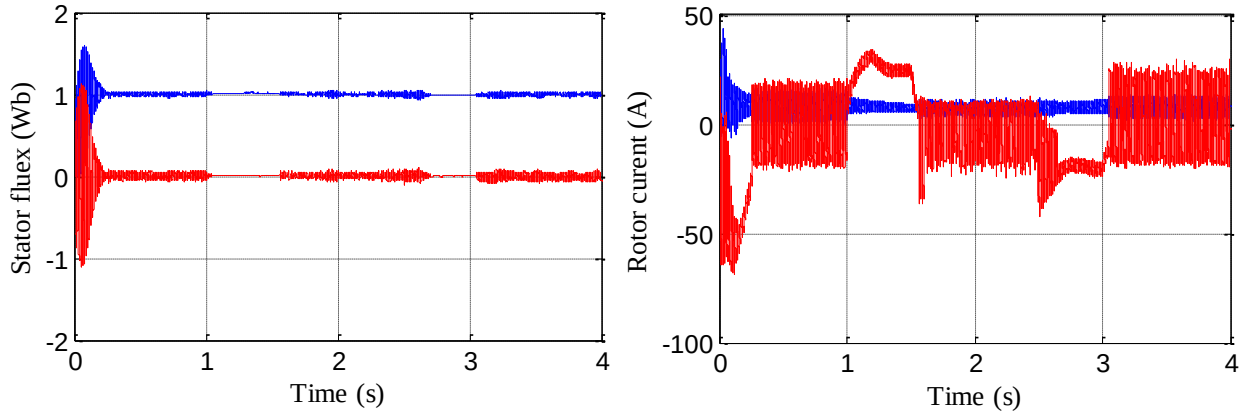

Figure (III.11): Simulation results during speed variation

III.8.3 Operation of the machine during rotor resistance variation

A +100% increase in rotor resistance is applied between t=1.5s and 2.5s, along with a load of $C_r = 15\,n.m$. The machine speed remains unchanged, torque and flux stay stable, and phase currents slightly increase in amplitude, showing the robustness of the SMC-PI-Fuzzy control.

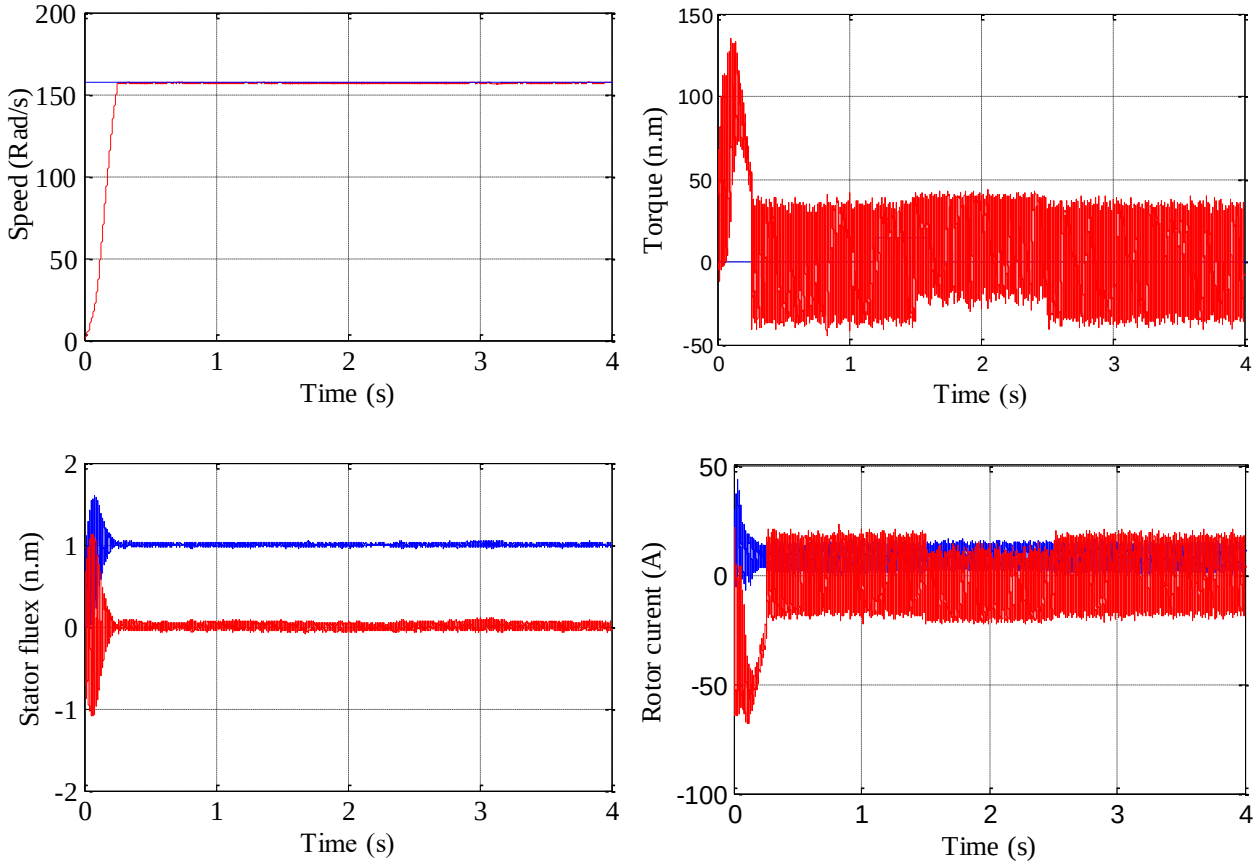

Figure (III.12): Simulation results during the variation of the rotor resistance.

III.8. 4Operation of the machine during stator resistance variation

A +100% increase in stator resistance R_s is applied between t=1.5 and 2.5 s. There are no changes in speed or flux, confirming the robustness of the SMC-PI-Fuzzy control against this variation.

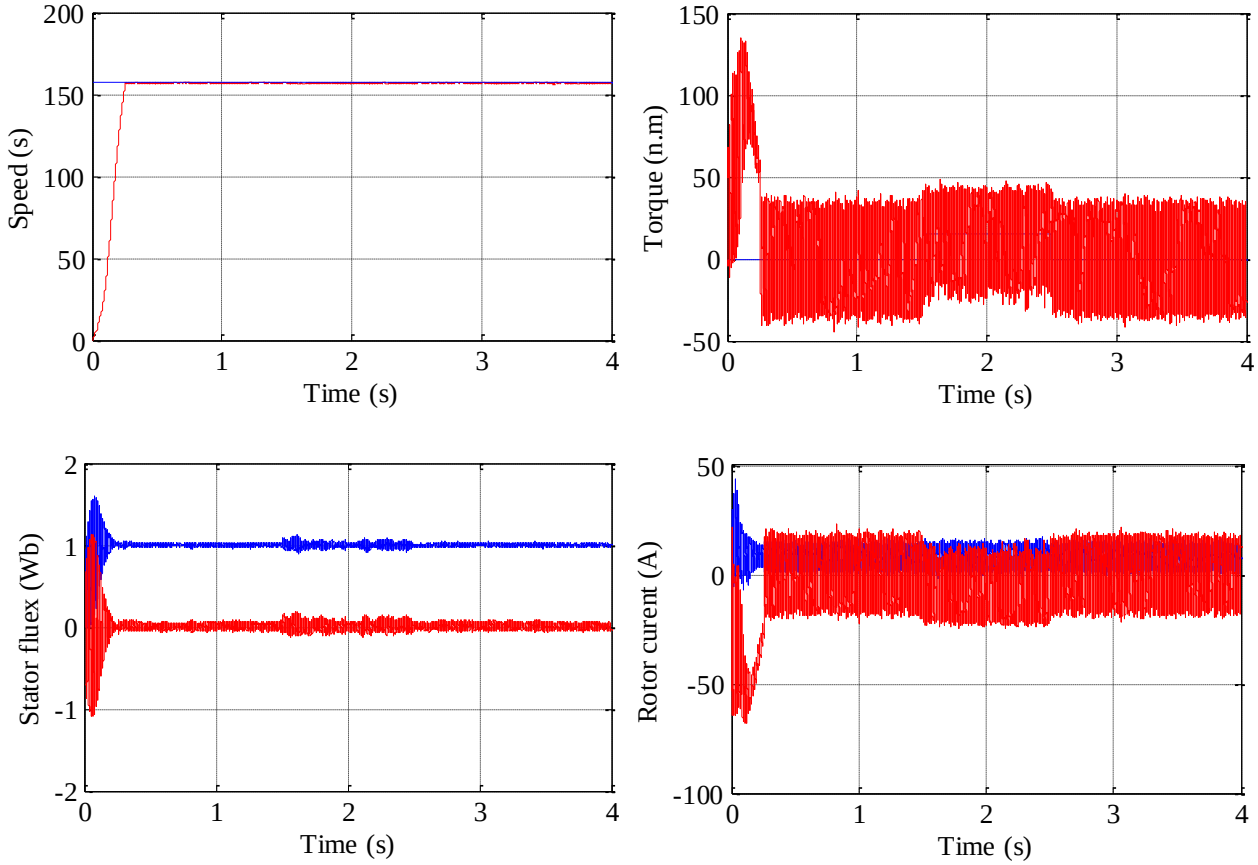

Figure (III.13): Simulation results during the variation of the stator resistance.

II.8.5 Interpretation of the results

The simulation results confirm the effectiveness of the hybrid SMC-PI-Fuzzy controller in improving the performance of the Doubly-Fed Induction Machine (DFIM). The rotor speed accurately follows the reference signal under various operating conditions including load variation, speed changes, and parameter disturbances with significantly reduced tracking error and faster settling time.

During load variation, the electromagnetic torque quickly adjusts to the applied resistant torque, while the speed remains stable and the flux shows minimal deviation. This demonstrates the controller's strong disturbance rejection capability. In speed variation scenarios, the controller enables smooth transitions between different speeds, including direction reversal, without noticeable oscillations.

When testing changes in rotor and stator resistance, the system maintained stability. Speed and flux were largely unaffected, with only slight increases in current amplitude. These results highlight the controller's robustness and adaptability to parameter uncertainties.

Overall, the hybrid control strategy successfully combines fast dynamic response, precise tracking, and high robustness, making it a reliable and efficient choice for advanced control of doubly-fed induction machines—clearly outperforming conventional methods.

III.9 Conclusion

In this chapter, the design, implementation, and performance evaluation of the hybrid control strategy FUZZY-SMC-PI have been comprehensively studied on the Doubly-Fed Induction Machine. This machine is considered a key component in renewable energy systems, especially in variable-speed wind turbines, due to its ability to operate efficiently across a wide speed range, along with good dynamic performance and reduced energy losses.

The proposed control strategy aims to enhance one of the most critical aspects of operating the DFIM, namely precise and reliable speed control. While traditional methods may suffer from shortcomings such as slow response, inability to eliminate steady-state error, or lack of robustness against external disturbances, the FUZZY-SMC-PI strategy provides an intelligent and balanced approach that combines the advantages of multiple control techniques.

This hybrid structure has demonstrated the ability to adapt flexibly to various operating conditions. The intelligent switching facilitated by fuzzy logic has improved system stability, reduced oscillations and overshoot, and shortened settling time, especially in scenarios involving sudden changes in load or reference speed.

Simulation results have shown that this strategy not only enhances speed tracking accuracy, but also mitigates the adverse effects commonly associated with traditional methods—such as chattering in SMC or slow response in PI control. The fuzzy supervisor has ensured smooth coordination between the two modes, resulting in optimal real-time performance.

Therefore, the FUZZY-SMC-PI strategy can be considered a robust and scalable solution for modern electric drive systems, particularly in applications requiring high dynamic performance and adaptability. Its implementation on DFIM opens broader horizons toward more efficient and intelligent renewable energy systems, with improved reliability under real-world operating conditions

General Conclusion

In the contemporary era of uninterrupted industrial advancement and the mounting reliance on electric machines in exacting and critical applications, there is an urgent requirement for effective control strategies that can effectively manage the nonlinear and dynamic behaviour of such systems. The doubly-fed induction machine (DFIM) is of particular significance due to its ability to regulate the flow of electricity in both directions, thereby ensuring high flexibility in the control of speed and power. This renders the DFIM an optimal candidate for utilisation in a variety of applications, including wind energy systems and advanced electric drives.

Nevertheless, the control of the DFIM is fraught with significant challenges, most notably its high sensitivity to parameter variations and the difficulty of maintaining dynamic performance under disturbances or fluctuating operating conditions. This research proposes an innovative solution through the development of a hybrid control strategy that combines three powerful techniques: The following controllers are considered: fuzzy logic, sliding mode control (SMC), and the proportional-integral (PI) controller.

The study commences with the construction of a detailed model of the DFIM, followed by an analysis of its electrical and mechanical behaviour through the utilisation of differential equations. The Park transformation is then employed to streamline the design of control algorithms. The implementation of vector control facilitates the decoupling of torque and flux components, thereby enabling enhanced precision in speed regulation.

The central tenet of this work lies in the integration of the three control techniques into a unified hybrid regulator. The proposed system capitalises on the robustness of SMC against disturbances, the simplicity and accuracy of PI control, and the adaptive intelligence of Fuzzy Logic, which dynamically tunes control parameters based on system conditions. This integration was not merely a technical implementation; rather, it was the culmination of a thorough analytical study, ensuring that each technique complemented the others within a coherent control structure.

The findings from the simulation exercise corroborate the efficacy of this hybrid approach. The controller demonstrated rapid and precise speed regulation, diminished settling time, and consistent operation in the presence of parameter uncertainties and load disturbances. The incorporation of fuzzy logic has been demonstrated to exert a considerable influence on the chattering phenomenon that is commonly associated with SMC, thereby enhancing the smoothness and quality of control signals.

What is particularly noteworthy about this work is that it goes beyond theoretical validation to include an in-depth practical evaluation through a comprehensive comparative study with previous academic works. These include graduation theses that addressed conventional control systems, such as the thesis ([Title of Thesis 1, Year]), the thesis ([Title of Thesis 2, Year]), and the thesis ([Title of Thesis 3, Year]).

The results of the comparison clearly demonstrate the superiority of the proposed hybrid controller in several key aspects, including faster response time, reduced settling time, improved tracking accuracy, and minimized ripple in the output signal—especially under varying operating conditions or sudden load disturbances. This reflects the flexibility and high performance of the proposed controller compared to conventional methods, which often show limitations in such challenging scenarios.

These findings signify not merely an incremental enhancement but a substantial scientific contribution to the domain of electric machine control, exemplifying the substantial advantages of integrating classical control with intelligent techniques.

This study opens promising perspectives for future developments, such as integrating neural networks, type-2 fuzzy systems, or adaptive intelligent regulators, to further increase system flexibility and autonomy in complex and evolving operational environments.

References

[1] Leonhard, W. “Control of Electrical Drives”, *Springer-Verlag*, 3rd Edition, 2001.

[2] Peña, R., Clare, J. C., & Asher, G. M. “Doubly fed induction generator using back-to-back PWM converters and its application to variable-speed wind-energy generation“, *IEE Proceedings - Electric Power Applications*, vol. 143, no. 3, pp. 231–241, 1996.

[3] Bose, B. K. Modern Power Electronics and AC Drives, *Prentice Hall*, 2002.

[4] Utkin, V. I. “Sliding mode control design principles and applications to electric drives,” *IEEE Transactions on Industrial Electronics*, vol. 40, no. 1, pp. 23–36, 1993.

[5] Zadeh, L. A. “Fuzzy sets,” Information and Control, vol. 8, pp. 338–353, 1965.

[6] R. Rouabhi, "Contrôle des puissances générées par un système éolien à vitesse variable basé sur une machine asynchrone double alimentée", Thèse de doctorat, Université Hadj Lakhdar, Batna, Algérie, 2016.

[7] DJ. Khodja, " commande des convertisseurs électromécaniques ", Polycopie De Cours, Master1, ISE, Université de M’sila, Algérie, 2012.

[8] M. M. Negm & T. M. Nasab, "Integral VSC and Preview Control of Efficiency and Speed for a DC Drive", Proceedings. International Conference on Power System Technology, Kunming, China, vol. 2, pp. 675-682, 2002.

[9] A. Arias, L. Romeral, E. Aldabas & M. Jayne, "Stator flux optimised Direct Torque Control system for induction motors", Electric Power Systems Research, vol. 73, no. 3, pp. 257-265, 2005.

[10] A. Zemmit, "Contribution à la commande de la machine asynchrone à double alimentation (MADA) par les techniques intelligentes", Thèse de doctorat, Université Mohamed Boudiaf, M’sila, Algérie, 2017.

[11 M. T. Cao, "Commande numérique de machines asynchrones par logique floue", Thèse de doctorat (PhD), Université Laval, Québec, Canada, 1997

[12] A. Masmoudi, A. Toumi, M. B. A. Kamoun & M. Poloujadoff, "Power on analysis and efficiency optimization of a doubly fed synchronous machine", Electric Machines and Power Systems, vol. 21, no. 4, pp. 473-491, 1993.

[13] G. Grellet & G. Clerc, "Actionneurs Electriques: Principes, Modèles, commande", Edition Eyrolles, 1999.

[14] M. Allam, B. Dehiba, M. Abid, Y. Djeriri & R. Adjoudj, "Etude comparative entre la commande vectorielle directe et indirecte de la Machine Asynchrone à Double Alimentation (MADA) dédiée à une application éolienne", Journal of Advanced Research in Science and Technology (JARST), vol. 1, no. 2, pp. 88-100, 2014.

[15] A. Khlaief, "Contribution à la commande vectorielle sans capteur mécanique des machines synchrones à aimants permanents (MSAP)", Thèse de doctorat, AIX-Marseille Université et l’École supérieure des sciences et techniques, Tunis, 2012.

[16] G. Salloum, "Contribution à la commande robuste de la machine asynchrone à double alimentation", Thèse de doctorat, Institut National Polytechnique, Toulouse, France, 2007.

[17] N. Abu-tabak, "Stabilité dynamique des systèmes électriques multimachines: modélisation, commande, observation et simulation", Thèse de doctorat, École Centrale de Lyon, France, 2008.

[18] K. Loukal, "Commande robuste des machines asynchrones à double alimentation à base des systèmes flous type deux", Thèse de doctorat, Université Mohamed Boudiaf, M'sila, Algérie, 2017.

[19] Ross, T. J. (2010). Fuzzy Logic with Engineering Applications. John Wiley & Sons.

[20] Math Works – Fuzzy Logic Toolbox: *https://www.mathworks.com/products/fuzzy-logic.html*

[21] Energy Procedia (Elsevier): Fuzzy logic-based control of doubly fed induction generator

[22] Open Classrooms – Introduction to Fuzzy Logic

[23] Timothy J. Ross, Fuzzy Logic with Engineering Applications, 3rd Edition, Wiley, 2010.

[24] George J. Klir and Bo Yuan, Fuzzy Sets and Fuzzy Logic: Theory and Applications, Prentice Hall, 1995.

[25] H.-J. Zimmermann, Fuzzy Set Theory—and Its Applications, 4th Edition, Springer, 2001.

[26] N. Bounar, A. Boulkroune, F. Boudjema, M. M'Saad & M. Farza, "Adaptive fuzzy vector control for a doubly-fed induction motor", Neurocomputing, vol. 151, no. 2, pp. 756-769, 2014.

[27] A. Bartoszewicz, "Sliding Mode Control", InTech, Croatia, 2011.

[28] U. Benz, "Réglage par mode de glissement hybride: appliqué au réglage de position de systèmes électromécaniques", *Thèse de doctorat, Ecole polytechnique fédérale*, Lausanne, Suisse, 1990

[29] J. J. E. Slotine & J. A. Coetsee, "Adaptive sliding controller synthesis for non-linear systems", *International Journal of Control*, vol. 43, no. 6, pp. 1631-1651, 1986

[30] S. Zeghlache, "Commande non linéaire d'un appareil à vol vertical", *Thèse de doctorat, Université Mohamed Boudiaf*, M'sila, Algérie, 2014

[31] R. Ouiguini, R. Bouzid & Y. Sellami, "Une commande robuste par mode glissant flou appliquée à la poursuite de trajectoire d'un robot mobile non holonome", *Conférence Internationale sur les Systèmes de Télécommunications*, d'Electronique Médicale et d'Automatique, Tlemcen, Alegria, 2003

[32] H. Amimeur, D. Aouzellag, R. Abdessemed & K. Ghedamsi, "Sliding mode control of a dual stator induction generator for wind energy conversion systems", *Electrical Power and Energy Systems*, vol. 42, no. 1, pp. 60-70, 2012.

[33] N. Hamdi, "Amélioration des performances des aérogénérateurs", *Thèse de doctorat, Université des Frères Mentouri*, Constantine, Algérie, 2013

[34] D. Kairous & R. Wamkeue, "DFIG-based fuzzy sliding-mode control of WECS with flywheel energy storage", *Electric Power Systems Research*, vol. 93, pp. 16-23, 2012

[35] Z. Chen and C. Chen, "A Hybrid PI-SMC-Fuzzy Controller for Nonlinear Systems," *Journal of Control Science and Engineering*, 2013

[36] Dr.H Abdelghafour, amélioration des performances de la commande non linéaire robuste d'un moteur asynchrone a doublé alimentation, Thèse de doctorat, Université Mohamed Boudiaf, M'sila, Algérie, 2021

[37] Haider A. F. Mohamed, E. L. Lau, S. S. Yang, M. University of Malaya Fuzzy-SMC-PI Flux and Speed Control for Induction Motors, 2008

Appendix

Parameters of the Doubly-Fed Induction Machine (DFIM)

C.1 Nominal Parameters

$P_n = 4\ KW$	Nominal Power
$v/U = 220\ 380V - 50Hz$	Nominal Voltage
$i/I = 15/8.6A.$	Nominal Current
$\Omega_n = 1440\ tr/min$	Nominal Speed
P =2	Number of Pole Pairs

C.2 Electrical Parameters

R_s= 1.2 Ω	Stator Resistance
R_r=1.8 Ω	rotor Resistance
L_s= 0.1554 H	Stator Inductance
L_r= 0.1568 H	rotor Inductance
M=0.15 H	Mutual Inductance

C.3 Mechanical Parameters

$j = 0.2\ Kg.m^2$	Moment of Inertia
$f = 0.001\ N.m.s/rd.$	Friction Coefficient.

Thesis submitted in partial fulfillment of the requirements for the Master 2 degree in Science in automatic and systemes

Topic:

Fuzzy - SMC - PI Regulator for Speed Control of the Doubly Fed Induction Machine

By: SAOUCHI Louey - BELABBES Fares

Abstract:

This thesis proposes a robust nonlinear control strategy for the Doubly-Fed Induction Machine (DFIM), combining PI control, Sliding Mode Control (SMC), and type-1 fuzzy logic. The goal is to improve system performance under variable speeds and loads. Various control methods, including vector control and SMC, were evaluated through simulations. Results confirm the dynamic advantages of the hybrid fuzzy controller in enhancing speed, torque, and flux regulation.

Keywords: DFIM, PI, SMC, FUZZY, VECTOR CONTROL**.**

Résumé:

Ce mémoire propose une stratégie de commande non linéaire robuste pour la machine asynchrone à double alimentation (MADA), en combinant la commande PI, la commande par mode glissant (SMC) et la logique floue de type 1. L'objectif est d'améliorer les performances du système sous des vitesses et des charges variables. Diverses méthodes de commande, y compris la commande vectorielle et SMC, ont été évaluées à travers des simulations. Les résultats confirment les avantages dynamiques du régulateur flou hybride en matière de régulation de la vitesse, du couple et du flux.

Mots clés: MADA, PI, MODE GLISSANT, LOGIQUE FLOUE, COMMAND VICTORIAL**.**

ملخص:

تقترح هذه المذكرة إستراتيجية تحكم غير خطي قوية للمحرك غير المتزامن مزدوج التغذية(MADA) ، من خلال دمج التحكم PI، والتحكم بطريقة الانزلاق(SMC) ، والمنطق الضبابي من النوع الأول. يهدف هذا العمل إلى تحسين أداء النظام تحت ظروف مختلفة من السرعة والحمولة. تم تقييم عدة طرق تحكم، بما في ذلك التحكم الاتجاهي وSMC، من خلال عمليات محاكاة. تؤكد النتائج على المزايا الديناميكية للمنظم الضبابي الهجين في تنظيم السرعة، والعزم، والتدفق.

الكلمات المفتاحية: الآلة غير المتزامنة مزدوجة التغذية ـ المنظم التناسبي-التكاملي ـ التحكم بطريقة الانزلاق ـ المنطق الضبابي ـ التحكم الاتجاهي (التحكم الشعاعي)